Scientific Contributions Oil & Gas, Vol. 49. No. 2, June: 81 - 111

SCIENTIFIC CONTRIBUTIONS OIL AND GAS

Testing Center for Oil and Gas
LEMIGAS

Journal Homepage:http://journal.lemigas.esdm.go.id
ISSN: 2089-3361, e-ISSN: 2541-0520

Structural Integrity Assessment of A Low Temperature Separation Unit (LTSU) Strainer Handle-Plate in Oil and Gas Operations: Coupled CFD and FEA Analysis of Fluid-Induced Loads

Mohd Azni Md Kasim[1], Mohd Azahari Razali[1], Norfakhira Mohd Nor[1], Iman Fitri Ismail[2], Masataro Suzuki[3], and Amnur Akhyan[4]

[1]Faculty of Mechanical and Manufacturing Engineering, Universiti Tun Hussein Onn, Malaysia, 86400 Parit Raja, Batu Pahat, Johor, Malaysia.

[2]Tuah Energy Sdn Bhd, T4-1-4, Tower 4, Maju Link, Bandar Tasik Selatan, 57000 Kuala Lumpur, Malaysia.

[3]Department of System Safety Engineering, Institute of GIGAKU, Nagaoka University of Technology, Nagaoka, Niigata, Japan.

[4]Politeknik Caltex Riau, Umban Sari No. 1, Umban Sari, Rumbai District, Pekanbaru City, Riau 28265, Indonesia.

Corresponding author: Mohd Azahari Razali (azahari@uthm.edu.my)

Manuscript received: February 05th, 2026; Revised: February 26th, 2026
Approved: March 04th, 2026; Available online: June 05th, 2026; Published: June 05th, 2026.

ABSTRACT - Structural strainers play a vital role in oil and gas processing facilities by removing solid contaminants from process fluids and protecting downstream equipment. In a Low Temperature Separation Unit (LTSU), a premature failure occurred at the handle punching plate connection of a strainer after approximately five years of continuous operation. This study aims to identify the root cause of the failure and to evaluate improved design configurations capable of withstanding operational loads. A coupled Computational Fluid Dynamics (CFD) and Finite Element Analysis (FEA) methodology was employed. CFD simulations were conducted to determine internal flow characteristics, pressure distribution, and pressure drop under both normal and contingency operating conditions. The resulting fluid-induced pressure loads were transferred to structural models for FEA to evaluate von Mises stress, displacement, strain, and unity check (UC) values for three designs with different punching plate thicknesses. The original design (Geometry A) exhibited high stress concentration at the handle–plate interface and UC values exceeding allowable limits, explaining the observed field failure. Geometry B showed improved performance under normal conditions but approached critical limits during contingency operation. Geometry C demonstrated the best structural integrity, maintaining UC values within acceptable limits in all cases while reducing peak stresses and deformation. The results confirm that insufficient plate thickness was the primary cause of failure and that increasing thickness significantly enhances structural reliability. The study demonstrates that the coupled CFD–FEA approach is an effective tool for failure diagnosis and design optimisation of process equipment subjected to fluid-induced loading in oil and gas operations.

Keywords: low temperature separation unit (LTSU), strainer failure, computational fluid dynamics (CFD), finite element analysis (FEA), oil and gas.

DOI org/10.29017/scog.v49i2.2033

How to cite this article:

Mohd Azni Md Kasim, Mohd Azahari Razali, Norfakhira Mohd Nor, Iman Fitri Ismail, Masataro Suzuki, and Amnur Akhyan, 2026, Structural Integrity Assessment of A Low Temperature Separation Unit (LTSU) Strainer Handle-Plate in Oil and Gas Operations: Coupled CFD and FEA Analysis of Fluid-Induced Loads, Scientific Contributions Oil and Gas, 49 (2) pp. 81-111. DOI org/10.29017/scog.v49i2.2033.

INTRODUCTION

Strainers are quite important equipment in pipeline systems, which are used to mechanically separate suspended particles in flowing fluids or gases (Akhyan et al., 2025). They use holes or net-like materials to sieve debris, thus amplifying the efficiency of operation and minimising the cost of maintenance. There are several designs, each of which is designed to reduce the pressure drop and easily clean the system, which is vital to ensure the integrity of systems. Strainer technologies have been developed to deal with challenges of performance, which include pressure drop, ease of maintenance and flexibility of changing fluid conditions. These advancements can be seen through different unique designs. Concave design of the strainer is incorporated with a smooth shell of a sphere together with a concave perforated plate, allowing for a large trapping area and minimal pressure drop across the strainer (Beattie et al., 1983). The strainer described in the paper utilises a circular, concave, perforated plate within a spherical shell to effectively remove debris from gas flow in a pipeline, minimising pressure drop while maximising the trapping area for particles (Beattie et al., 1983). The wrappable mesh strainer incorporates a straining mesh that can be rolled to expose fresh material, effectively capturing foreign particles while maintaining fluid flow (Bruchet & Kanno 2019). A strainer, as described in the paper, utilises a wrappable straining mesh to mechanically remove foreign particles from fluid introduced through an inlet, allowing clean fluid to flow out through an outlet after filtration (Bruchet & Kanno 2019). The omega type of the design minimises flow channel transformation and maximises screening surface area, enhancing operational efficiency and ease of maintenance (Kim 2009). The strainer described in the paper utilises an omega-type screen to filter foreign objects from fluid, preventing malfunctions in machinery and pipelines. It features a straight-line inlet and outlet, enhancing operational efficiency and ease of maintenance (Kim 2009).

In addition to the mechanical issues of filtration, new strainers offer physical operational advantages that directly result in the economics and reliability of systems. The benefit of less energy loss is one of the major ones. One of the most important aspects when it comes to pipeline operations is energy efficiency, and the choice of strainer also contributes a lot to the maintenance of optimal hydraulic performance (Akhyan et al., 2025). Strainers like the in-line pipeline strainer are designed to minimise energy loss, which can significantly lower operational expenses (Rea et al., 1984). The paper describes a pipeline strainer featuring first and second perforated conical sheet metal walls, designed to remove particles from fluid flow. It includes a removable strainer element for maintenance, ensuring effective filtration within the pipeline system (Rea et al., 1984). Some strainers include features like air release valves and baffles to manage entrained gas and debris, ensuring smoother operation (Richter & Martin 2017). Yes, a strainer is a device that uses a straining element to mechanically remove particles from a flowing fluid or gas in a pipeline, as described in the research paper, which details a pipeline strainer with various features (Richter Martin 2017). Strainers are a crucial device of the modern pipeline system because they offer mechanical filtration, minimise equipment failures, and enhance the efficiency of work. Design innovations. These include concave plates, wrappable mesh elements, as well as omega-type screens and indicate continuing developments in the way of improving the performance of filtration whilst reducing loss of pressure. Nevertheless, their performance can be controlled to ensure that their overall performance is optimised through close attention to the behaviour of fluids, the behaviour of particles, and system working conditions. Ongoing strainer design research will help provide more efficient, reliable and flexible fluid processing systems.

The low temperature separation unit (LTSU) strainer is very important in the efficient separation of gas elements, especially in petrochemical processes. It is optimised to work in low temperatures, which makes it easy to eliminate impurities and allows a higher level of purity of the gas being separated. The LTSU normally has a completion of structural constituents that streamlines its functionality, such as a cylinder body, demisters, and multiple discharges of gas and liquid substances. The working of the LTSU strainer is directly associated with its structural design, which is designed in such a way that it leads to a higher rate of phase separation and eliminates blockages during low temperatures of operation. The major arrangement of the LTSU is a vertical cylinder body, into which the internal separation elements are set. The LTSU typically features a vertical cylinder with a tangential inlet for material, a flushing prevention baffle, and a demister to separate gas from liquid (Zhang & Xiao 2012). The arrangement of components, such as the demister above the baffle, optimises gas flow and separation efficiency (Zhang & Xiao 2012). The paper describes a low-temperature separator featuring a flushing prevention baffle and a demister, which are crucial for efficient gas-liquid separation in petrochemical processes, ensuring effective separation of liquefied gas components within the cylinder body (Zhang & Xiao 2012).

The LTSU strainer is used in processing low-temperature gas, which is inefficient in terms of operational efficiency. The LTSU utilises a low-temperature method of taking advantage of variations in condensation and freezing points of gas mixtures. This is quite useful in dehydrating natural gas, separating hydrocarbons, and condensate materials. The low-temperature processing allows achieving high separation power with minimal chemical treatment, which improves the overall performance of the plant (Zhu et al., 2022). Second, wax management by the oiling technique. One of the operational problems that LTSUs face is low-temperature wax precipitation. A new mitigation process is to inject oil into the system that will reduce the precipitation temperature of the wax. This ensures a lower chance of wax deposition, none of the strainer and related pipelines is blocked, and it allows continuous and safe operation (Zhu et al., 2022). There is an initial implication of cost in the application of advanced operation strategies, especially the oiling process to manage the aspect of the wax. Nevertheless, in the long-term, there are proven economic gains in spite of the fact that the initial investment is significant. The method enhances the reliability of the system, minimises unplanned failures, increases the service life of equipment, and alleviates the expenses of maintenance related to the removal of wax (Zhu et al., 2022). Consequently, the practices lead to better performance in the lifecycle and overall profitability of its operation. On the other hand, although the LTSU strainer is practical, problems like the deposition of wax in low temperature conditions may hamper the operation. To solve these problems and make LTSUs more efficient overall, constant improvements in design and operational methods are needed (Zhu et al., 2022).

The modern oil and gas processing facilities have low-temperature separation units (LTSU) as part of them. Their main role is the effective separation of hydrocarbons at low temperatures, which is a process necessary in optimising the extraction and purification of natural gas liquids (NGLs). Through their effectiveness in separation, LTSUs ensure high recovery of valuable hydrocarbons and work to reduce the use of energy and cut down total operational expenses. Their design and use point to the industry consideration of efficiency, safety, and economic viability.

The dynamics of LTSUs lie in the fact that their success in operations is based on the accurate control of thermodynamic and fluid dynamic laws. Diphlegmation and fractionation are some of the processes commonly used in these units to separate the lighter hydrocarbons and the heavier components. The incoming gas stream is, in practice, cooled first in recuperative heat exchangers. The condensation of the hydrocarbons is also caused by this cooling, and it is then collected and separated using low-temperature separators (Vladislavovich 2019). Utilising fractionation columns, the lighter hydrocarbons are separated from heavier components. The process is enhanced by recycling condensed vapours to improve efficiency and reduce refrigeration needs (Currence 2016). Enhanced LTS processes require less refrigeration while achieving higher recovery rates of valuable hydrocarbons. This is accomplished through advanced designs that minimise compression requirements and optimise energy use (Currence 2016; Kurochkin 2020). The paper describes the enhanced low temperature separation (LTS) process reduces refrigeration needs while maximising recovery of heavier hydrocarbons. It utilises an absorber and de-ethanizer tower, achieving efficient separation with less compression compared to conventional LTS processes, ensuring product quality. The temperature and pressure inside LTSUs are very sensitive, and the slightest deviation may affect the performance of the separation process and the quality of products greatly.

LTSUs provide significant benefits from an economic perspective. Conventional hydrocarbon separation processes can be characterised by high energy requirements, but LTSUs can also achieve similar or higher separation efficiency with less energy use, which is directly converted into the low cost of operation (Zhu et al., 2022). Besides technological achievements, like the integration of oiling processes, also improve the unit performance, reducing wax deposition, which is a typical operation issue that may hinder the flow and affect equipment integrity (Zhu et al., 2022). Although LTSUs, along with their design and installation, can be expensive, the benefits can be extremely high in the long run, even though the initial capital cost may be substantial, because the technology ensures greater recovery of hydrocarbons, energy efficiency, and less maintenance.

To sum up, low-temperature separation units are a hallmark of effective hydrocarbon processing in the oil and gas industry (Nursyifa 2017). Using state-of-the-art cooling, condensing, and separation methods, LTSUs optimise the yield of useful NGLs and reduce energy costs and other operational inefficiencies. Their application is important in contemporary hydrocarbon processing, even though it involves careful planning and requires a lot of investment, the operational and economic returns justify it. With the industry still geared towards sustainability and efficiency, LTSUs will still be a vital technology towards the quest to extract resources in an optimised manner.

The fundamental difference between the two computational methods of engineering design, that is, between the Computational Fluid Dynamics (CFD) and the Finite Element Analysis (FEA) is the aspect of their specialisation and the problem they are supposed to address. The behaviour of fluids, liquids, and gases and the phenomena of fluid flow, turbulence, pressure distribution and heat transfer are the main concerns of CFD. This renders CFD critical in the analysis of components or systems where the fluid flow is a dominating factor, e.g. in pipelines, compressors, gas turbines, heat exchangers and aerodynamics. Mechanically, on the contrary, FEA is concerned with how solid structures behave in response to different forms of loading. It studies the stress distribution, deformation, vibration properties, and possible failure modes to make sure that the parts will be able to sustain the conditions of operation in a safe and reliable way. CFD is especially useful when an engineer needs to know about the finer aspects of the fluid flow in or around a system. It is able to display velocity profiles, pressure drops and temperature gradients that enable designers to assess the efficiency and performance of fluid-dependent processes. As noted by Hadebe et al. (2024), CFD offers sufficient information about the behaviour of fluids in various situations at the boundaries. Moreover, in fluid mechanics-based systems, like gas turbines, the CFD tools are essential in optimising the combustion performance, cooling methods and the entire performance of the system (Amirante et al., 2012). Conversely, FEA is the methodology to use in the evaluation of the structural integrity of components. It allows engineers to model the behaviour of materials to mechanical forces, pressure, vibration and thermal expansion. Hadebe et al. (2024) have suggested that FEA is used to determine the ability of a component to withstand the operational stresses without collapsing. FEA is essential in complex mechanical systems like turbochargers, where it is used to determine the life of fatigue, structural deformation prevention, and safety at high rotational speeds and varying loads (Luczynski et al., 2019).

The use of CFD and FEA as a combination is increasingly becoming important to modern engineering design, where algorithms like fluid flow and structural response are strongly coupled. The latest developments in the field of simulation technology have provided the capability to perform thermal coupling, in which the temperature fields calculated using CFD can be input into FEA models to determine the resulting thermal stresses. Sun et al. (2008, 2010) showed that an iterative data exchange of temperature and heat flux between the CFD and FEA is an effective means of improving the accuracy of simulation of complex thermal interactions. It is particularly essential in systems with a high temperature like gas or steam turbines, where fluid behaviour and structural capabilities affect the general performance and stability (Amirante et al., 2012). In spite of the fact that coupled simulations are more complete and realistic in their predictions, there are situations when uncoupled methods can be the best. In cases where computational facilities are scarce or where the interplay between fluid and structure is not so strong that complete modelling is of little extra use, engineers can decide to perform CFD and FEA independently. Uncoupled approaches, as Luczynski et al. (2019) observe, can affect accuracy in some way, although they allow quicker analysis, which can also be worthwhile in the case of initial design or when a quick iteration is required. Finally, CFD and FEA play different but significant roles in engineering design, and the knowledge of their differences, including the way these tools can be combined, will enable engineers to choose the best one to use in every stage of analysis.

The Low Temperature Separation Unit (LTSU) strainer plays a very crucial role in the stability and security of downstream processing procedures, especially in the gas handling and separation systems. One of the LTSU strainers suffered a structural failure five years after being in continuous service. The fault was found on the upper part of the unit, at the point of connection of the punching plate and handle structure. The image in Figure 1 shows the damaged strainer. This is a local failure, which indicates the possibility of mechanical strength weakness, design constraints, and unexpected operational loads, which are beyond the initial design expectations. It also poses safety hazards, downtime in operations, as well as potential system contamination in case debris or broken parts get into the downstream equipment. Since several of the strainers in the system are designed and operate in the same way, it is imperative to research whether this operational mechanism is exclusive or systemic. In order to avoid recurrence, a thorough analysis that combines both fluid behaviour and structural response must be conducted. This will assist in the identification of the failure mode, be it due to the abnormal distribution of pressure, excessive pressure drop, cyclic stresses, fatigue, or poor material strength. This kind of understanding is essential in defining the corrective measures, design modifications and maintenance measures to improve the level of reliability of every LTSU strainer in service.

Figure 1. Strainer conditions during operation show catastrophic failure, leading to debris pass-through and potential downstream component damage.

The main goal of this research is to properly investigate the performance and structural integrity of the Low Temperature Separation Unit (LTSU) strainers of SP22-2112, 2119, 2222, and 2229 strainers with a view to trying to figure out what might have led to the failure observed. This involves carrying out extensive CFD simulations to examine the fluid flow behaviour with special focus on assessing the pressure distribution and in determining the nature of pressure drop based on each strainer model. Simultaneously, the paper would measure the mechanical strength of the strainer components through the performance of Finite Element Analysis (FEA) under loading conditions of fluids. Structural assessment is aimed at checking the rates of Von Mises stress, displacement, and strain of the individual parts and unit tests that determine whether the parts are working within the reasonable safety margins or not. These analyses will give a complete picture of the performance of the strainers and suggestions on how to enhance the design integrity and prevent failure of the strainers in future.

METHODOLOGY

In this section, the general methodology used in the investigation of the structural failure which took place in the connection between the handle and plate of the punching of the LTSU strainer is described. The method is a combination of both FEA and CFD in order to encompass the effects of fluid loading and the structural response. CFD simulations were performed to model the flow behaviour of oil and gas fluids within the LTSU strainer under operational conditions. CFD is initially used to study the pressure distribution and pressure drop properties, then, the loads forced by the fluid are studied in an FEA system to determine Von Mises stress, displacement, strain, and unit check. Material properties were defined based on the low-temperature operating environment typical in oil and gas processing, ensuring accurate prediction of brittle or fatigue-prone behaviour (Sunarjanto et al., 2017).

The failure of the LTSU strainer involves both fluid behaviour and structural response, requiring analysis of fluid-structure interaction effects. CFD was used to determine the pressure distribution and pressure drop within selected LTSU strainers, while FEA was applied to evaluate structural integrity under the resulting fluid-induced loads in terms of Von Mises stress, displacement, strain, and unity check. The combined CFD–FEA approach provides a comprehensive and cost-effective method for identifying failure mechanisms in complex pipeline components where experimental testing is limited.

The structural failure of the Low Temperature Separation Unit (LTSU) strainer involves coupled fluid and mechanical effects, requiring analysis of both flow behaviour and structural response. The integration of Computational Fluid Dynamics (CFD) and Finite Element Analysis (FEA) offers a robust framework for evaluating complex systems like the LTSU strainer. CFD excels in simulating fluid flow, capturing velocity fields, pressure distributions, and turbulence characteristics through numerical methods that solve the Navier-Stokes equations (Gülich 2014); Schmidt 1987). Conversely, FEA focuses on structural integrity, assessing stress, strain, and deformation under various loading conditions (Odabaee et al., 2014). By combining these methodologies, engineers can transfer fluid-induced forces from CFD to FEA, enabling a comprehensive analysis of both fluid dynamics and structural responses.

CFD provides detailed insights into flow phenomena, essential for understanding internal dynamics in enclosed systems (Li et al., 2024). It allows for analysis without physical alterations to the system, making it ideal for complex geometries (Nakayama, n.d.). FEA evaluates how structures respond to fluid forces, calculating critical parameters like stress and displacement (Odabaee et al., 2014). Accurate input data from CFD enhances the reliability of FEA results, ensuring realistic assessments of safety factors (Schmidt 1987). While the CFD-FEA approach offers a comprehensive evaluation, it is important to note that the accuracy of both methods heavily relies on the quality of the input data and the assumptions made during modelling.

While both methods offer significant advantages in design optimisation and performance prediction, they also come with notable disadvantages that can impact their effectiveness in certain applications. CFD limitations include being computationally intensive, requiring significant processing power and time, especially for complex simulations (Computational Fluid Dynamics, n.d.). Results can be sensitive to mesh quality and boundary conditions, potentially leading to inaccuracies (bakker & marshall, n.d.). While FEA limitations such as may not accurately capture fluid -structure interactions unless coupled with CFD, which can complicate the analysis (Sun et al., 2009), it requires extensive validation against experimental data to ensure reliability, which can be resource-intensive (Li et al., n.d.). While CFD and FEA are invaluable tools in modern engineering, their limitations necessitate careful consideration of their application contexts. In some cases, simpler analytical methods may suffice, particularly when computational resources are constrained or when rapid assessments are needed.

Simulated strainer geometry

The geometry of the simulated strainers is composed of a series of connected conical (simulated strainer) that are permeable to sizable particles (such as carbon fibre or other porous materials) but not smaller particles. The geometry of the simulated strainers is made up of a series of connected conicals (simulated strainer), which are permeable to large sized particles (diameters of carbon fibre or other porous materials) but not smaller particles. The physical structure and configuration of the LTSU strainer is digitally constructed to reflect its physical structure and operational set-up. The geometry comprises a mesh screen, a ring plate and a punching plate such that all the aspects affecting the flow behaviour and structural loads are captured correctly. Both CFD and FEA simulations are based on this geometry model and permit a consistent understanding of fluid forces and structural performance that can be used across domains.

Original geometry

The original geometry of the LTSU strainer is as shown in Figure 2. This geometry was obtained from the design specifications and includes key features such as the mesh screen, ring plate, and punching plate. The geometry has been redrawn in SOLIDWORKS to accurately reflect the modifications and to facilitate the CFD and FEA simulations. The changes in the thickness of the punching plate are depicted in the redesigned model. For the purpose of simulations, the following modifications have been made to the strainer. These three variants are hereby referred to as Geometry A, Geometry B, and Geometry C, as shown in Figure 3.

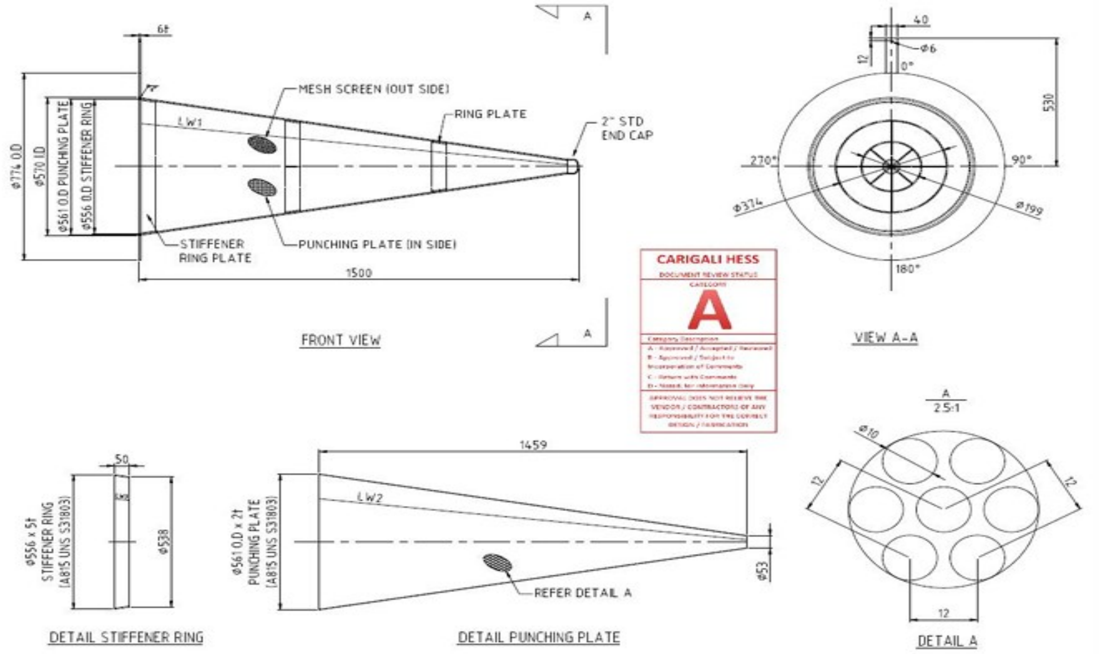

Figure 2. The strainer technical drawing, shows the design specifies an A815 UNS S31803 duplex stainless steel punching plate, providing a high strength-to-weight ratio and superior resistance to chloride stress corrosion cracking compared to standard 300-series steel.

Table 1. Strainer geometry for simulation

Geometry	Modification	Remark
A	Unmodified, original model	Punching Plate Thickness = 6 mm
B	2 mm increase in the punching plate thickness	Punching Plate Thickness = 8 mm
C	4 mm increase in the punching plate thickness	Punching Plate Thickness = 10 mm

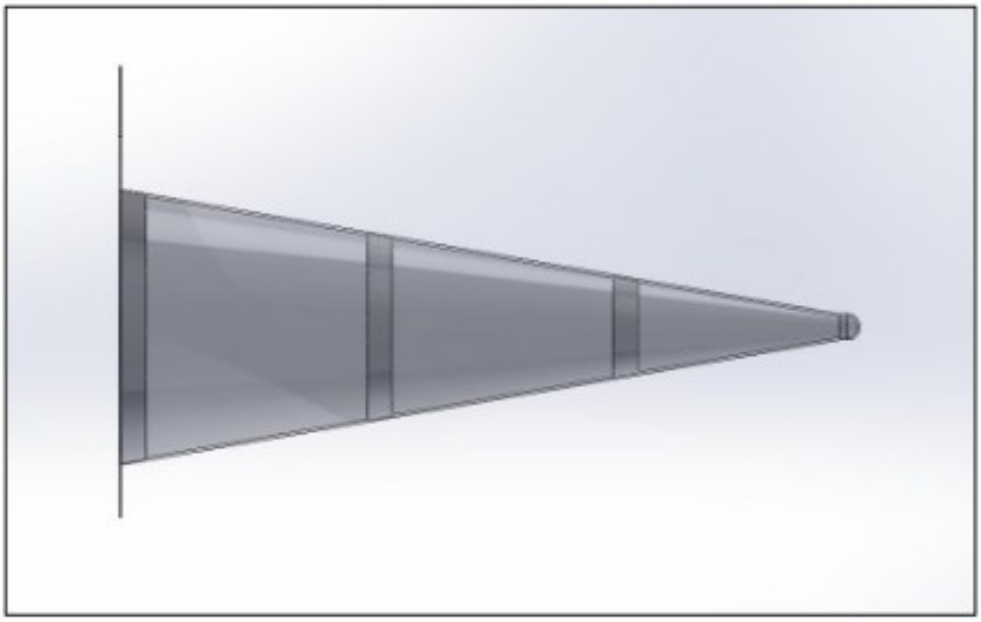

Figure 3. The strainer model for Geometry A, B, and C in SOLIDWORKS shows the conical shape is specifically engineered to reduce pressure loss and prevent excessive vortex formation, as confirmed by CFD simulations.

Strainer porous media

Calculation for the opening area of the strainer is based on data in 3.2.11_Book 100 of 170_Strainer Dossier. Figure 4 shows data for strainer porous media. Figure 4 provides quantitative validation for strainer design. It calculates the Total Initial Pressure Drop (ΔPi) at 0.0656 barG, ensuring that the strainer provides enough filtration (122% opening area ratio) without causing an unacceptable loss in system pressure during startup.

Fluid properties

The thermophysical properties of the fluid used in the analysis are extracted from the following PCHE datasheet (Table 2). PCHE stands for printed circuit heat exchanger.

Calculated thermophysical properties

The following thermophysical properties have been calculated from the PCHE Datasheet to support the CFD and FEA analyses of the LTSU strainers to determine the specific heat at constant volume (Cv), specific heat ratio (Cp/Cv), and molecular mass.

Standard case P = 30.51 bar g, T = 94.3 °C

Table 3. Thermophysical properties for standard case

Property	Value	Unit
Specific heat ratio (Cp/Cv)	1.202	-
Molecular mass	0.02897	kg/mol
Dynamic viscosity	0.000016	Pa*s
Specific heat (Cp)	1706	J/kg*K
Thermal conductivity	0.0370	W/(m*K)

Table 2. Flow parameters from printed circuit heat exchanger (PCHE) data sheet (Akhyan et al., 2025)

DS-H2205-9	PCHE DATA SHEET		Sheet 5 of 8
Operator	Carigali Hess Operating Company Sdn Bhd	Project	Cakerawala booster compression project
Contractor	Hyundai Heavy Industries	Project No	402025-00889
Enquiry/Order No	PO: QE532B2Q66	Item No(s)	CKX-E-2104-2144-2204-2244-2184
Equipment	1st Stage Aftercooler	No. of items required	5
Case	Case 3: HMB Case HP 3 x 33% (P = 30.51 bar g)	Parallel sections per item	N/A

	Service per item	Side A				Side B				Rev
1	FLUID CONDITIONS	In		Out		In		Out		
2	Fluid	Hydrocarbon Gas				Cooling Water				
3	Flow rate, total (kg/hr)	653219 [NOTE 3]				682450 [NOTE 3]				
4	Flow rate, gas/vapour (kg/hr)	653219		650475		0		0		
5	Flow rate, liquid (kg/hr)	0		2744		682450		682450		
6	Temperature (°C)	94.3		40.5		33.0		55.0		
7	Design temp: (max/min) (°C)	160 / -29				160 / -29				
8	Pressure: inlet/design (barg)	30.5 / 38.0				4.6 / 16.0				3
9	Pressure drop: calc/allow (bar)	0.85 / 1.03				0.74 / 1.03				
10	FLUID PROPERTIES	Liq	Vap	Liq	Vap	Liq	Vap	Liq	Vap	
11	Density (liq/vap) (kg/m³)	–	29.0	828	35.4	995	-	986	-	
12	Specific heat (J/kg·K)	-	1706	3153	1688	4181	-	4181	-	
13	Viscosity (cP)	-	0.0160	1.984	0.0140	0.769	-	0.517	--	
14	Thermal conductivity (W/m·K)	-	0.0370	0.2320	0.0310	0.6213	-	0.6477		
15	Dew point (°C)									
16	CONNECTIONS									
17	No. of nozzles	1		1		1		1		
18	Nozzle size (mm NB)	600 NB		600 NB		300		300		
19	Flange class	Cl 300 RF		Cl 300 RF		Cl 300 RF		Cl 300 RF		
20	Max strainer aperture (microns)	320				320				
21	MATERIALS									
22	Nozzle material	UNS S31803		UNS S31803		UNS S31803		UNS S31803		
23	Flange material	UNS S31803		UNS S31803		UNS S31803		UNS S31803		
24	Header material	UNS S31803		UNS S31803		UNS S31803		UNS S31803		

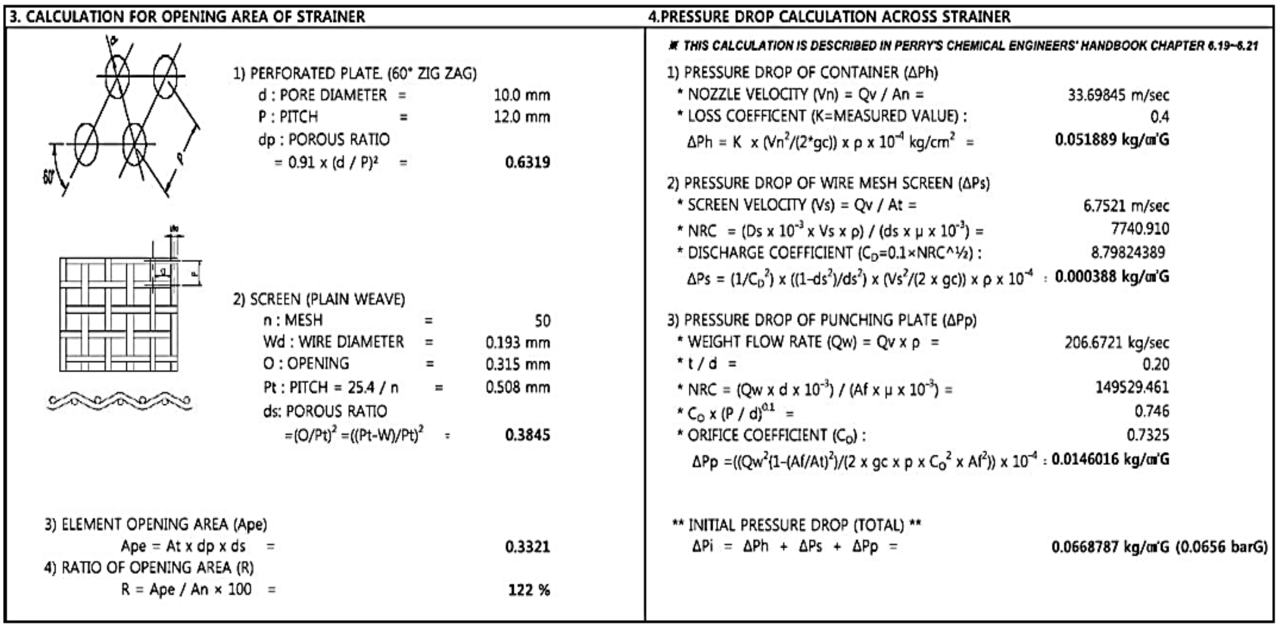

Figure 4. Calculation for opening area of strainer

Contingency case P = 36.61 bar g, T = 113.16 °C

Table 4. Thermophysical properties for contingency case

Property	Value	Unit
Specific heat ratio (Cp/Cv)	1.236	-
Molecular mass	0.02546	kg/mol
Dynamic viscosity	0.000016	Pa*s
Specific heat (Cp)	1706	J/kg*K
Thermal conductivity	0.0370	W/(m*K)

Boundary conditions

The initial and boundary conditions at the inlet and outlet of the strainers refer to the flow condition as specified in the PCHE Datasheet, as shown in Table 5. Actual condition is hereby referred to as (Case 1). Simulating contingency is a common practice to account for uncertainties and to identify potential risks and weaknesses in the current design. Therefore, the actual condition with 20% increase in fluid temperature and pressure is hereby referred to as (Case 2).

Table 5. Boundary conditions for case 1 and case 2

Boundary conditions	Case 1: Actual value	Case 2: Contingency	Unit
Inlet flow rate	653219	783862.8	kg/hr
Outlet flow rate	650475	780570	kg/hr
Inlet fluid pressure	30.51	36.6	Bar g
Temperature	94.3	113.16	°C

CFD mesh

A computational mesh is generated for the fluid domain to perform a CFD simulation. Mesh quality is ensured to capture pressure and flow distribution around the strainer and handle. Figure 5 shows the CFD mesh of the strainer for geometries A, B and C.

FEA mesh

The finite element analysis (FEA) mesh used for the structural analysis of the LTSU strainer is described below. The mesh was generated to ensure high-quality resolution of the structural features, enabling accurate simulation of stresses, displacements, strain, and UC. Figure 6 below shows the FEA mesh applied to the LTSU strainer.

Table 6. Mesh quality metrics

Mesh quality metrics	Value	Remarks
Max element size	97.4mm	None
Min element size	4.87mm	None
Total nodes	88,340	None
Total elements	43,659	None
Max Aspect Ratio (AR	75.483	None
% of Elements with AR <3 = 97.86	97.86 %	Fulfilled FEA mesh criteria
% of Elements with AR > 10	1.07%	Fulfilled FEA mesh criteria

The majority (97.86%) of elements have an AR lower than 3, indicating equilateral meshes with lower numerical errors, as shown in Figure 7.

Item	Mesh Display
Geometry A, B, and C	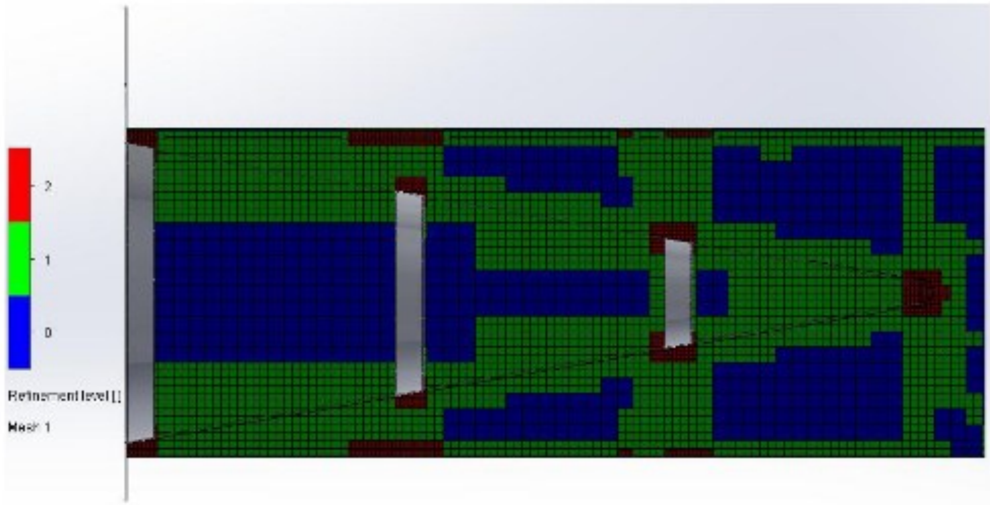

Figure 5. The CFD mesh of the strainer for geometries A, B, and C shows the mesh density has been refined (red zone) near the narrow flow channels and distal tip to better capture the high velocity gradients and local pressure effects critical for performance validation.

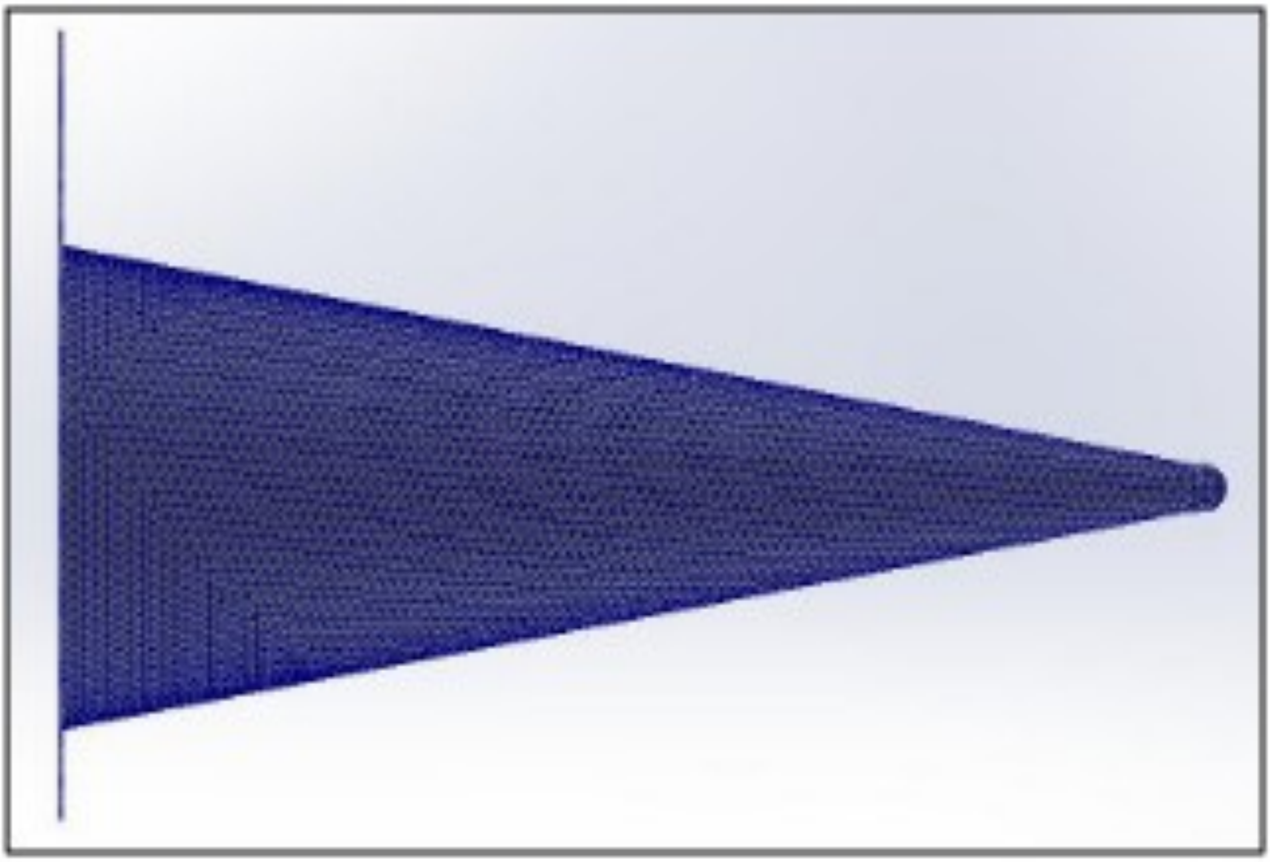

Figure 6. This figure displays a blended-curvature mesh, where the element size is automatically adjusted based on local geometric complexity.

RESULT AND DISCUSSION

Pressure distribution and pressure drop

The three results of pressure-drop of the three strainer geometries, such as A, B, and C, represent how the design differences affect the resistance of the fluid-flow under both the Standard Case (Case 1) and Contingency Case (Case 2) operating conditions, as shown in Table 6.

Geometry A as shown in Figure 8 will be considered as the reference baseline of both cases, where the average pressure drops will be 6233.61 Pa (Case 1) and 9361.48 Pa (Case 2) at strainer punching plate thickness = 6 mm. Actual condition is hereby referred to as (Case 1). Simulating contingency is a common practice to account for uncertainties and to identify potential risks and weaknesses in the current design. Therefore, the actual condition with 20% increase in fluid temperature and pressure is hereby referred to as (Case 2). These baseline values represent the natural behaviour of the original design, where Case 2 has much more intense pressure losses as it is under more adverse contingency conditions, like higher flow rate or high fluid density. As predicted, the minimum pressure and maximum pressure difference in Geometry A also show the same trend, which decreases from case 1 at about 5985.64-6794.11 Pa to case 2 at 8468.88-10610.30 Pa. Case 1 shows that the pressure distribution is relatively uniform across the strainer body. The legend indicates a pressure range from approximately 3.04 MPa (blue) to 3.07 MPa (red). The plot shows a gradual transition of colors, primarily dominated by green and yellow hues in

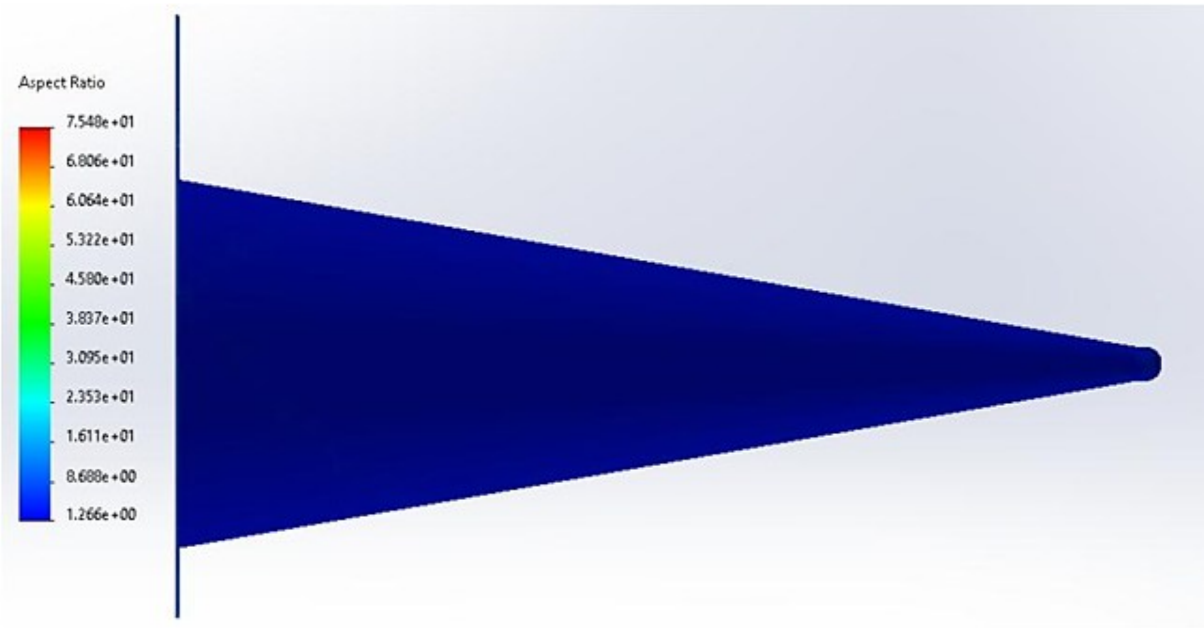

Figure 7. Aspect ratio (AR) of the strainer

Table 7. Pressure drop for geometry A, B and C

Geometry	Case	Unit	Pressure drop	Averaged pressure drop	Minimum pressure drop	Maximum pressure drop	Percentage change in averaged pressure drop (%)
A	1	[Pa]	6794.1127	6233.6127	5985.6360	6794.1127	Baseline (6233.6127 Pa)
	2	[Pa]	9144.7638	9361.4759	8468.8778	10610.3041	Baseline (9361.4759 Pa)
B	1	[Pa]	5903.8971	6511.4571	5800.3610	7363.4831	4.46
	2	[Pa]	10466.1333	9271.2820	8474.0993	10552.3552	0.96
C	1	[Pa]	7064.3532	6889.0058	6569.0559	7201.3949	10.51
	2	[Pa]	10247.0719	9281.4746	9215.6833	10579.5611	0.85

the conical section, suggesting stable flow. There are minor localized pressure drops (indicated by cooler colors) immediately downstream of the internal stiffener rings, but the overall gradient remains low. In Case 2, the pressure values are significantly higher, ranging from approximately 3.67 MPa to 3.69 MPa. The distribution is much more dynamic and non-uniform. There is a prominent blue low-pressure zone concentrated in the center of the cone between the second and third stiffener rings, indicating high-velocity flow or turbulence. The pressure gradients near the outlet (the tip of the cone) are much sharper than those in Case 1, showing intense high-pressure zones along the outer walls. Geometry B, as shown in Figure 9, shows a significant rise in pressure drop as compared to Geometry A at strainer punching plate thickness = 8 mm. Actual condition is hereby referred to as (Case 1). Simulating contingency is a common practice to account for uncertainties and to identify potential risks and weaknesses in the current design. Therefore, the actual condition with 20% increase in fluid temperature and pressure is hereby referred to as (Case 2). In Case 1, the averaged pressure drop increases to 6511.46 Pa, which is an increment of 4.46 percent of the baseline. This implies that the changes in design in Geometry B add to the resistance to flow, perhaps because of a changed layout of perforation, or limited flow area or constraints of geometry on streamlines. The impact is greater with Case 2, in which the averaged pressure drop rises to 9271.28 Pa, yet this equates with a 0.96 increase on the contingency baseline. This means that Geometry B acts more like Geometry A in cases of extremes when the characteristics of the flows would stabilise because the inertial effects are overpowering. Case 1 shows that the pressure

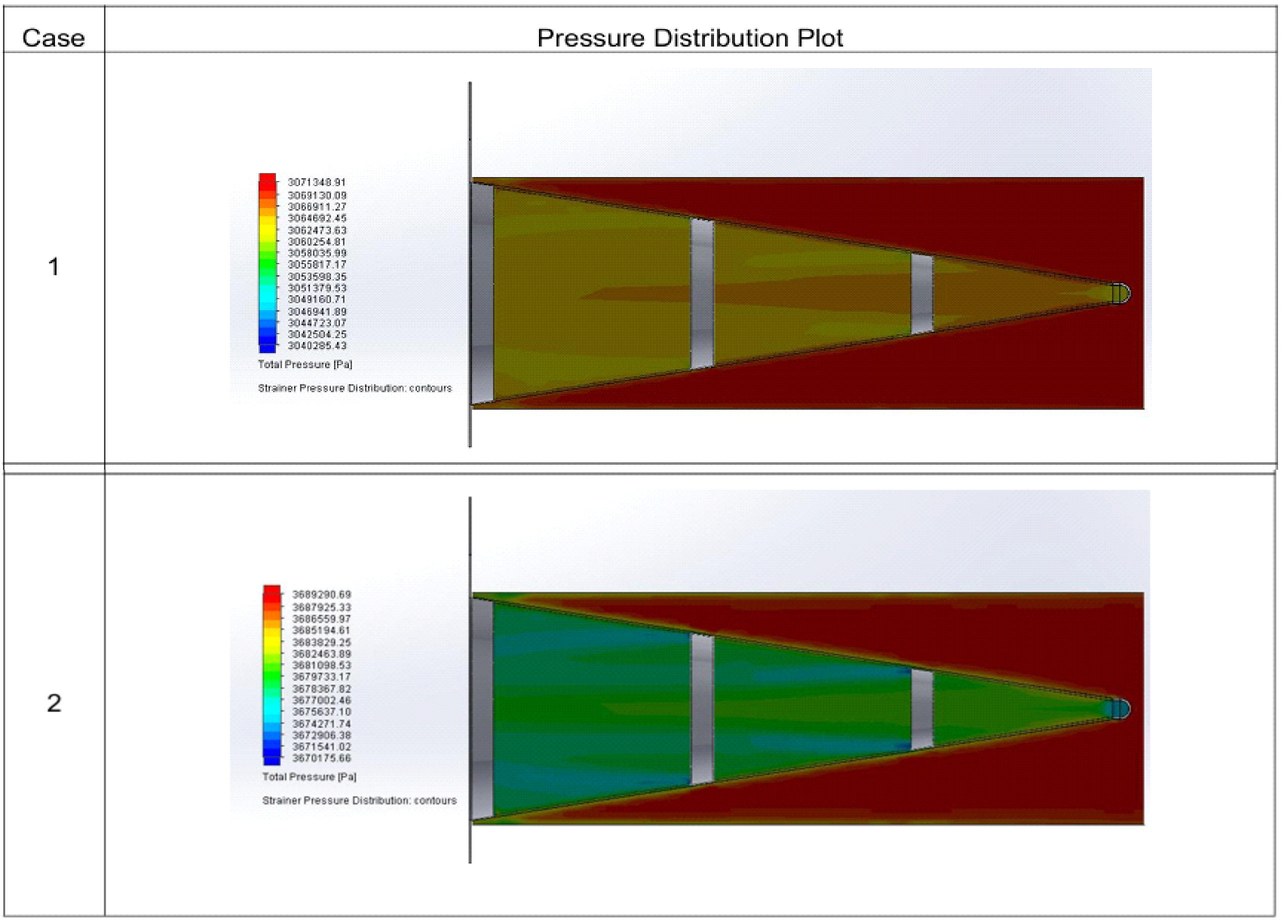

Figure 8. The pressure distribution plot for Geometry A at a strainer punching plate thickness of 6 mm. Geometry A, as shown in Figure 9, is considered the reference baseline for both cases, where the average pressure drops are 6233.61 Pa (Case 1) and 9361.48 Pa (Case 2) at a strainer punching plate thickness of 6 mm. The actual condition is hereafter referred to as Case 1.

distribution plot exhibits a relatively stable and uniform profile. The legend indicates a total pressure range from approximately 3.04 MPa to 3.07 MPa. The interior of the strainer is dominated primarily by yellow and light orange contours, suggesting a consistent pressure field with minimal fluctuations. There are subtle green streaks near the internal stiffener rings, indicating minor localized pressure drops as the fluid bypasses these structural elements. Although the overall visual pattern in Case 2 appears similar to that of Case 1, the scale is significantly different. The pressure range for this case is higher, between 3.67 MPa and 3.69 MPa. The contours within the conical section show a slightly more pronounced green-to-yellow gradient, particularly around the central axis and the second stiffener ring. This suggests that, although the flow remains relatively controlled, the higher operational pressure begins to concentrate stress near the narrower section of the cone.

Under Case 1, geometry C, as shown in Figure 10, exhibits the greatest dispersion of performance of pressure drops at strainer punching plate thickness = 10 mm. Actual condition is hereby referred to as (Case 1). Simulating contingency is a common practice to account for uncertainties and to identify potential risks and weaknesses in the current design. Therefore, the actual condition with 20% increase in fluid temperature and pressure is

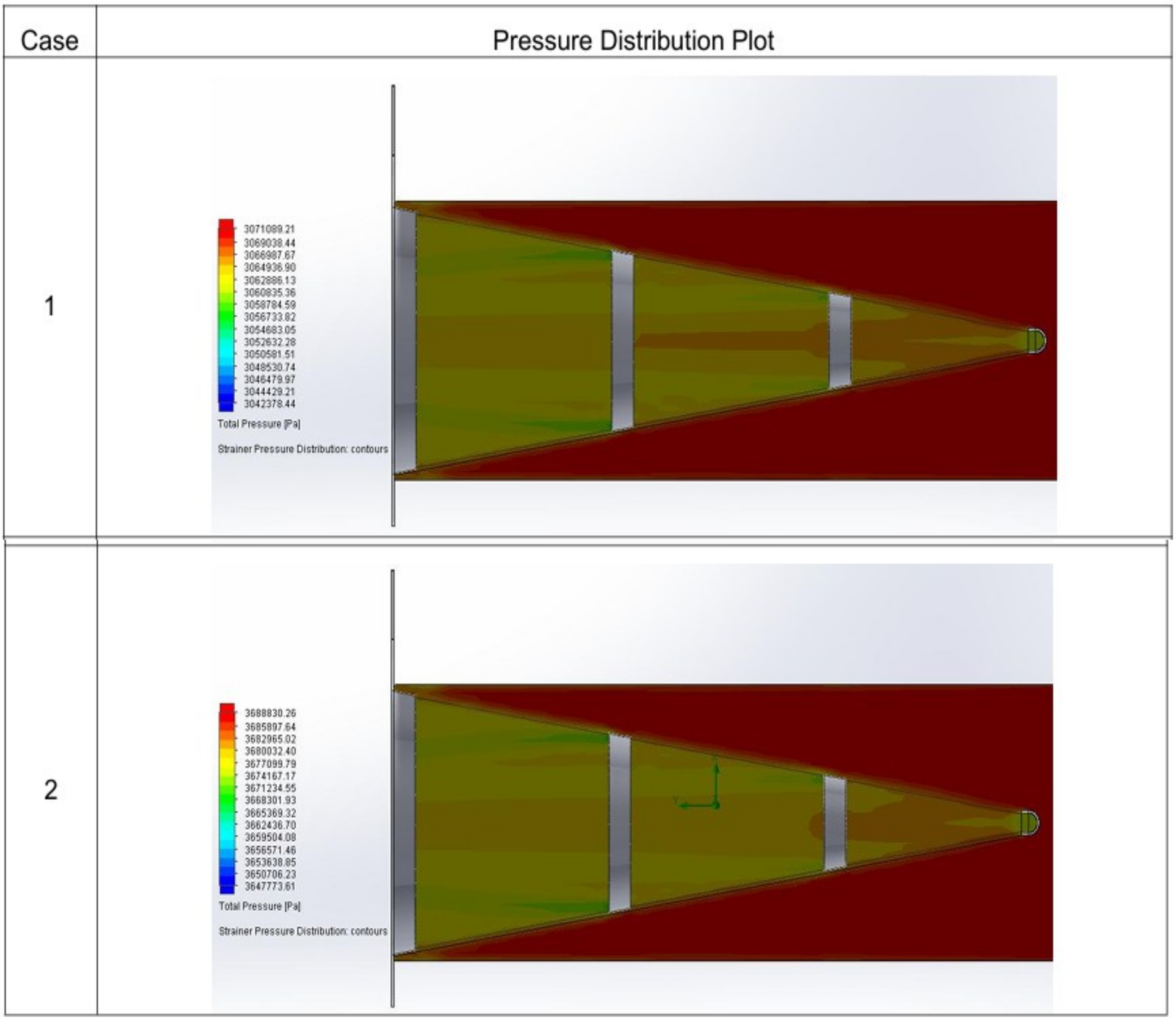

Figure 9. The pressure distribution plot for Geometry B at a strainer punching plate thickness of 8 mm shows a slight increase in pressure drop compared with the baseline, indicating that the increased plate thickness (8 mm) introduces moderate flow resistance while maintaining a relatively stable pressure distribution.

hereby referred to as (Case 2). Geometry C has the lowest resistance to the flow with an average pressure drop of 6889.01 Pa in the Standard Case, which increases by 10.51 percent compared to the baseline, the lowest efficient design of the three geometries. This large enhancement suggests that the changes which have been made to Geometry C introduce purposeful constraints on fluid motion, including more limited perforation compliance or more turbulence regions. In Case 2, however, the average change in pressure drop of 9281.47 Pa causes the change of only 0.85 percent over the base value. As in Geometry B, the influence of geometrical differences decreases in importance under the conditions of high stress, when the properties of fluids and the loads acting on them take overall control of the flow behaviour. . Case 1 shows that the pressure distribution exhibits a highly stable profile, with a total pressure range from approximately 3.04 MPa to 3.07 MPa. The interior of the strainer is almost entirely uniform in olive-green and orange, indicating very low pressure differential across the conical section. The streaks of lower pressure (green) observed in thinner geometries are nearly absent here, suggesting a very smooth fluid–structure interaction. In Case 2, the pressure range increases to approximately 3.64 MPa to 3.69 MPa. Despite the higher load, the distribution pattern remains nearly identical to Case 1. The flow appears to be well guided by the 10 mm plate, with no signs of central turbulence or low-pressure regions that were present in Geometry A. The pressure is consistently maintained along the strainer walls right up to the apex of the cone.

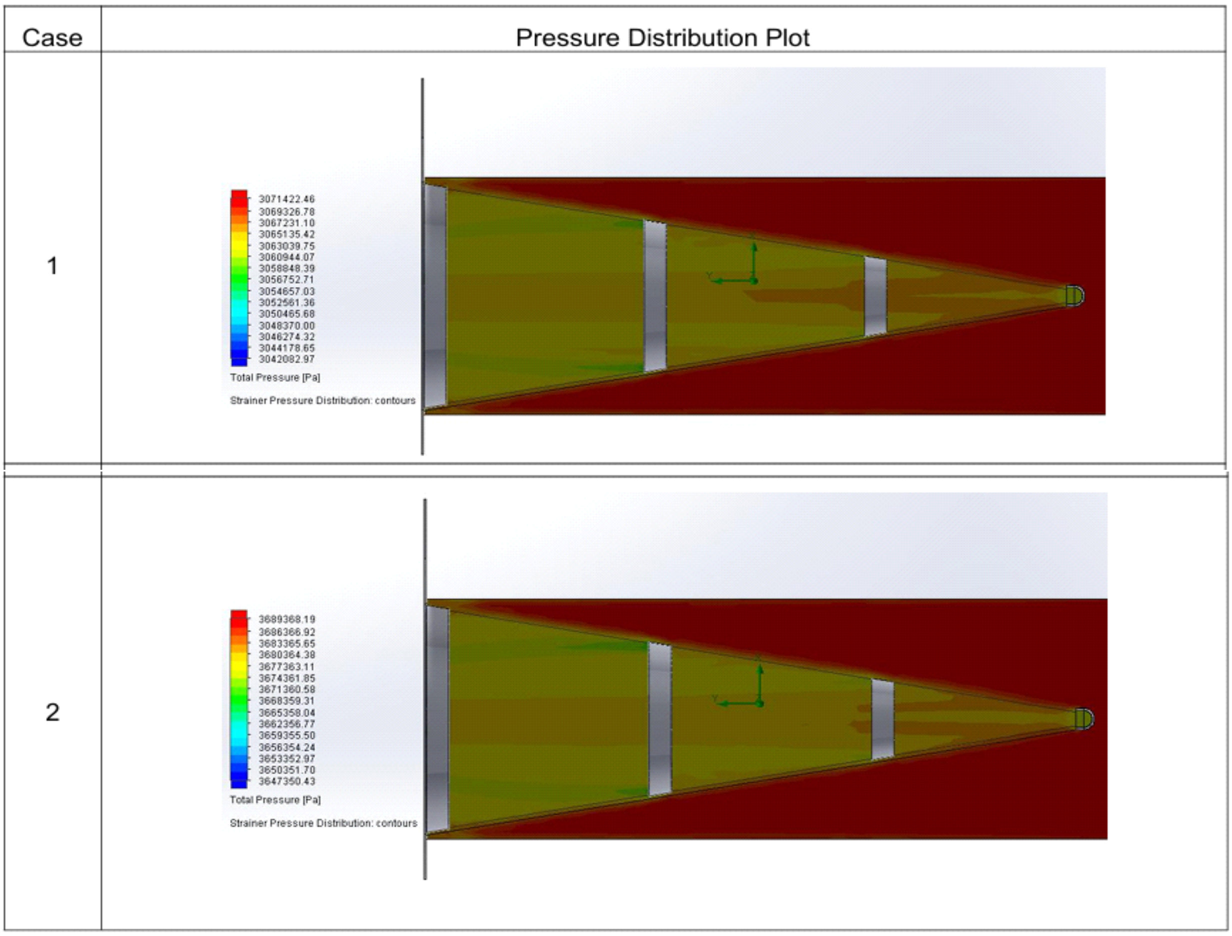

Figure 10. The pressure distribution plot for Geometry C at a strainer punching plate thickness of 10 mm demonstrates the highest pressure drop under normal operating conditions, suggesting that the 10 mm thickness significantly alters the flow behavior while improving flow uniformity and stability.

Table 7 provides the description of the pressure drop features of three geometries (A, B and C) in two operational cases, where Geometry A is the original design. The validity of the CFD simulation is based on the baseline values. In Case 1, the baseline pressure drop is 6233.6127 Pa, which is very close to the averaged pressure drop of Geometry A at 6233.6127 Pa. The baseline pressure drop of 9361.4759 Pa in Case 2 corresponds to the averaged pressure drop at Geometry A, and this is another argument towards the accuracy of the model. This comparison confirms to the fact that the CFD simulation of the original geometry is validated, and, consequently, the numerical model is reliable to represent the real -life hydraulic behaviour of the strainer. The validation is important because it would mean that the future CFD predictions of modified geometries B and C can be relied on. Therefore, the percent changes of the averaged pressure drop in Geometries B and C can give substantial information regarding the design changes in relation to hydraulic performance of the tested confirmed original design.

In conclusion, the comparison of geometries provides that all the modified designs (B and C) demonstrate greater pressure loss in comparison with the baseline, but their influence differs depending on the operating situation. Geometry C changes the most under people's operating conditions, whereas both B and C are nearer to the baseline performance under contingency conditions. The findings are crucial in determining the effectiveness of geometric changes in enhancing the structural robustness and hydraulic performance without undermining it too much.

Von mises stress, displacement and strain of geometry A of the case 1 and case 2 at strainer punching plate thickness = 6mm

The Finite Element Analysis (FEA) output of Geometry A under Case 1, as shown in Figure 12 and Case 2 as shown in Figure 13, operating conditions, gives an insight into the behaviour of the handle plate assembly to the loads exerted by the fluid due to fluid CFD results at strainer punching plate thickness = 6 mm. Actual condition is hereby referred to as (Case 1). Simulating contingency is a common practice to account for uncertainties and to identify potential risks and weaknesses in the current design. Therefore, the actual condition with 20% increase in fluid temperature and pressure is hereby referred to as (Case 2). The three important outputs of von Mises stress, displacement and strain point to the manner in which the structure responds to normal pressure loading conditions of the LTSU system.

The von Mises stress contour plot shows that most of the handle-plate structure is at very low levels of stress, which is represented by the heavy presence of dark blue areas. This implies that, in general, there is not so much stress on the geometry with Case 1 loading. Nevertheless, localised areas of high strains in the form of green and yellow lines are located around the connection area between the handle and the plate. Such concentration of the stresses is probably due to geometric discontinuities, such as sharp edges, transition of thickness, or weld interfaces. Though the stress levels in these focal areas are also not very high as compared to normal material yield limits, these focal areas are the signs of potential weak areas where long-term cyclic stress loading may start fatigue or may eventually result in cracking. The pattern of stress is in line with the real point of failure reported in the service, which supports the applicability of the simulation.

The displacement plot shows the way the structure will deform due to the pressure load. As predicted in the case of a cantilever-type geometry, the displacement progressively intensifies into the free end of the handle, and the largest deformation is at the tip. This is depicted through the development of colours of contours as dark blue at the fixed end, and orange or yellow at the free end. Even though the values of absolute displacement are insignificant (the range is 10-9 to 10-6 m), the pattern of deformation gives a valuable clue to the manner in which the load is carried along the structure. The even distribution means that the structure behaves without any problem due to the maturity of the structure, which can support Case 1 loading without the threat of overbending or instability. Nevertheless, a minor deformation can add to stress cycling in very important junctions during repeated functioning cycles.

Item	FEA Plot
vonMises Stress	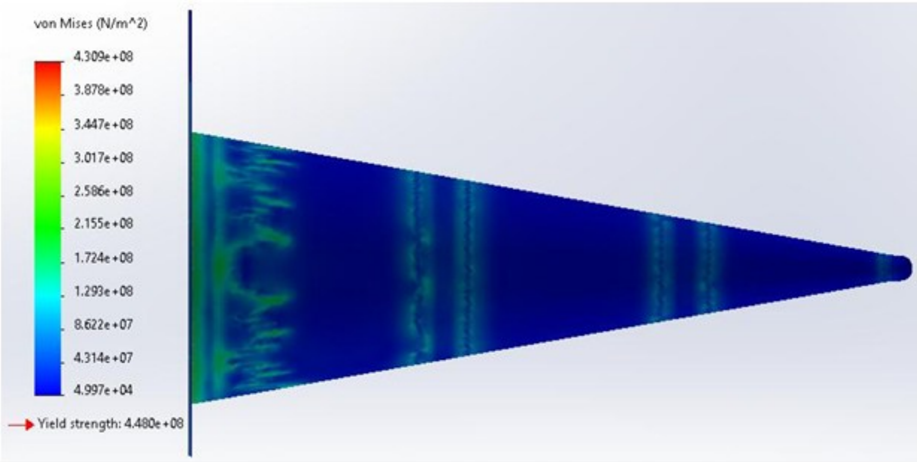
Displacement	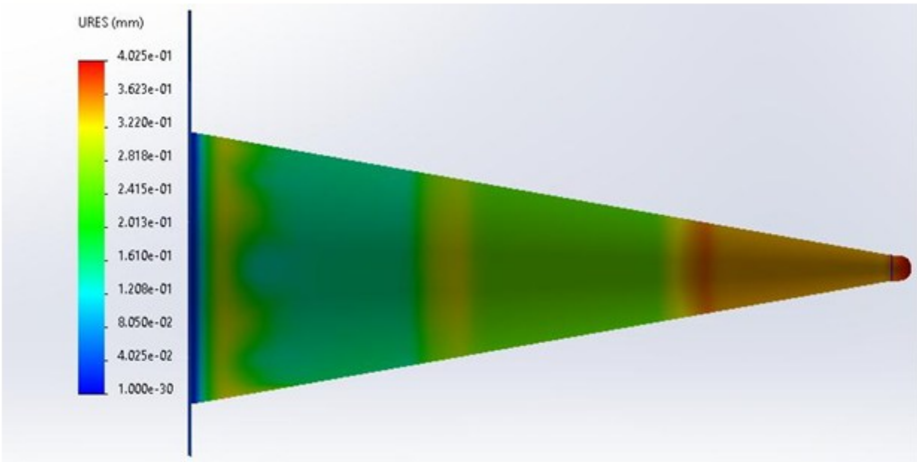
Strain	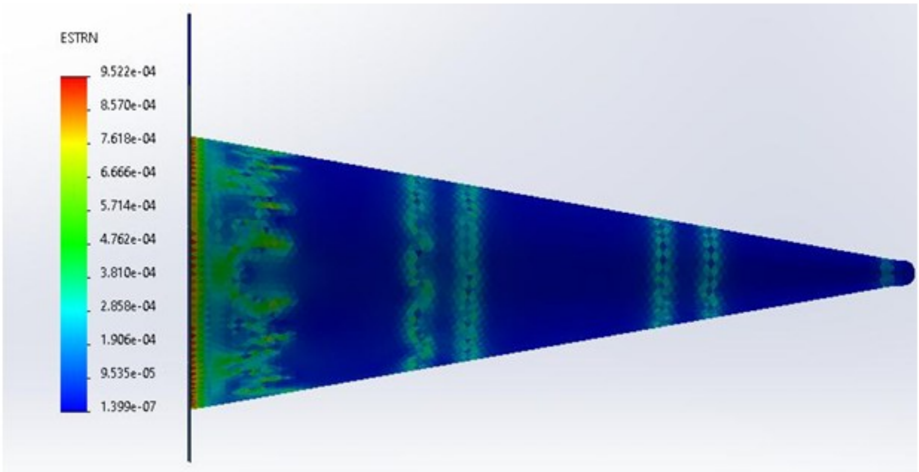

Figure 11. The FEA plot for Geometry A – Case 1 indicates low overall stress and deformation under normal operating conditions,with localized stress concentration at the handle–plate junction, which highlights a potential fatigue initiation point.

The trends are also evidenced by the strain plot in the distribution of stress. There is little strain in the bulk of the structure, as occurs in the deep-blue areas that prevail. Localised strain changes are observed around the connection area and along areas that have slight bending. These increased strain bands, like the von Mises stress results, are associated with geometric complexity areas, so the strain response depends more on shape transitions than on the overall intensity of loading. Though the strain values are not very high in number, the locations of the strain concentrations may become relevant in the presence of the cyclic pressure loads or fluctuating pressure loads, which may lead to the fatigue of the material in the course of time.

In conclusion, the FEA outcomes of Geometry A in Case 1 conditions show that the component will be subjected to low overall stress and deformation. The stress and strain concentration around such a junction at the handle level remains, however indicating that this area is prone to structural weakness. The results can be used to understand the reasons behind the real failure in this field and consider additional design additions to minimise the stress concentrations, load redistribution, and increase the structural durability in the long run.

Case 2, as shown in Figure 12, is the contingency or abnormal operating condition within the LTSU system, and in most cases, it is the increased pressure or sudden changes in the flow. Case 2 von Mises stress contour indicates that the magnitude of stress is evidently greater than that of Case 1. Whereas most of the structure lies in the low-stress blue spectrum, the fact that there are larger areas that are shifting to green, yellow and even light-orange colour is evidence of more stress on the component. These are high stresses that are mainly found around the area of connection between the handle plate, which agrees with the known area of failure. The increase in stress on this area with increased pressure loading indicates that this joint is more prone to increases in the load. Considering contingency conditions, such concentrations of stress may become critical over repetitive cycles, which may lead to a high likelihood of fatigue cracking or structural collapse.

In the plot of the displacement, when the Case 2 conditions are used, the deformation is noticeably greater than in Case 1. The transition of the blue gradient into the red is more intense, and the greatest distance displacement is observed at the end of the handle. This is not surprising since when the pressure loads are greater, the bending effects are also greater along the structure. The amplified deformation shows the increasing flexibility or way in which the component is vulnerable to deflection as the loads increase. Although absolute displacement values can yet remain within tolerable ranges, the greater the deflection, the more stress cycles at the fixed point of connection with each cycle. This increases the possibility of fatigue failure of the structure during changing loads or during extended duty.

The strain distribution is of the general trend observed in the stress and displacement plots, whereby higher strain levels are realised in Case 2. The connection region and the regions with more bending are represented by the contour map with more rich green and turquoise areas. These high values of strain indicate that as pressure loads are applied to the material in higher than normal operating conditions, larger deformations are experienced. Since strain is directly linked with material fatigue and plastic deformation, the results clearly demonstrate that the component is more threatened during contingency operations. The strains reveal points where the microstructural damage can be accumulated over time, which may result in an accelerated cracking or weakening process of the weld or joint interface.

The FEA outcome of Geometry A in Case 2 proves that contingency operating conditions are much more demanding to the structure than normal operation. Stress, displacement and strain are all augmented, especially in the handle-plate joining spot, the same area where the real-life structural failure took place. The conclusion is thus credited by the simulation that the initial design would not be stable when exposed to high load conditions. These results highlight the improvement in designs, including plate thickness, weld strength or geometry to decrease stress concentration and increase load distribution in abnormal operation conditions.

Item	FEA Plot
vonMises Stress	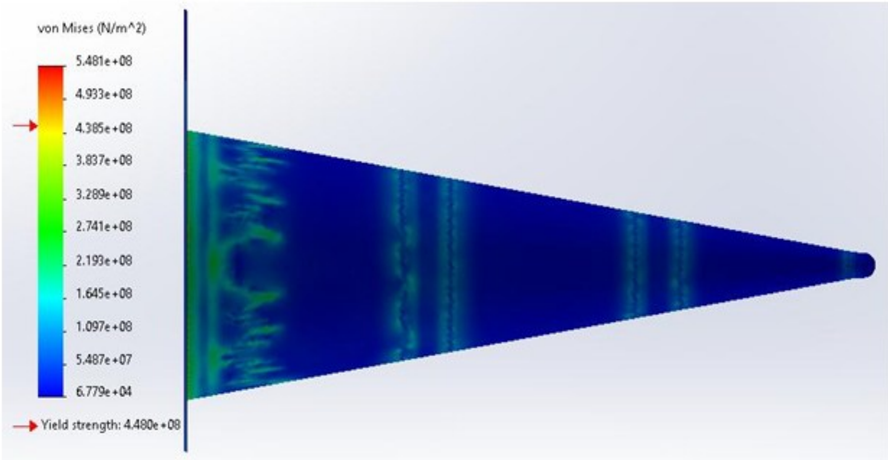
Displacement	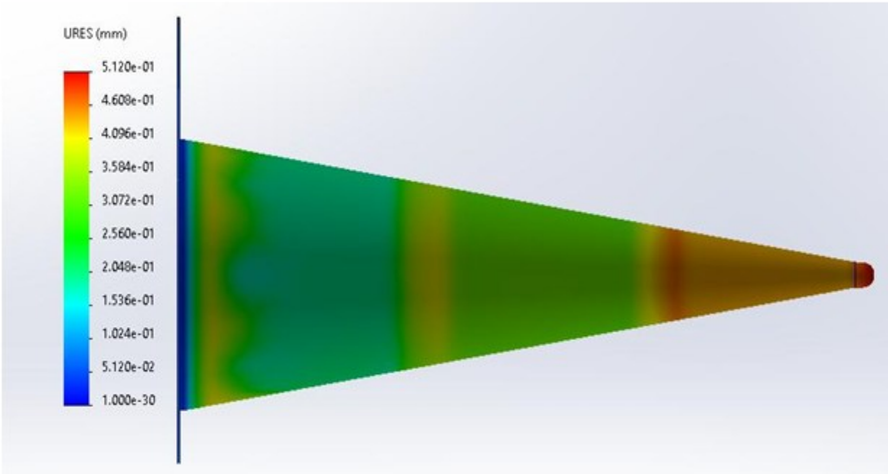
Strain	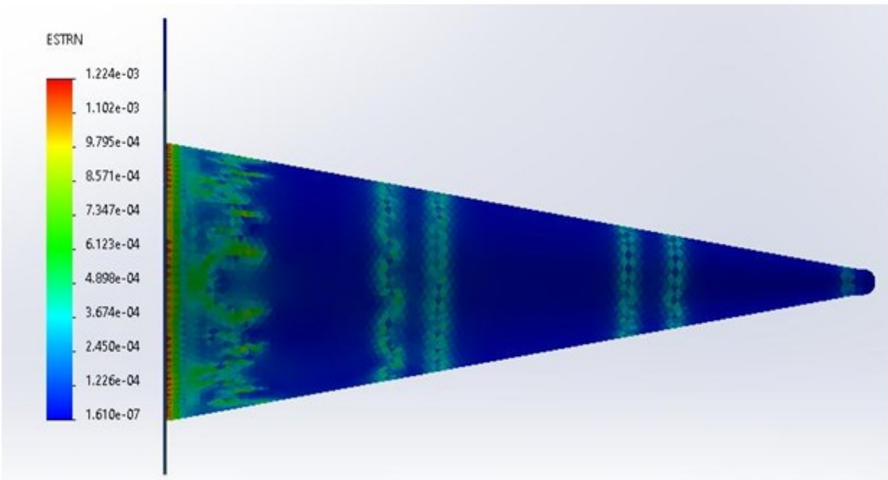

Figure 12. The FEA plot for Geometry A – Case 2 shows increased stress, displacement, and strain under contingency operating conditions, confirming that the handle–plate junction is highly susceptible to failure under increased loading conditions.

Von mises stress, displacement and strain of geometry B of the case 1 and case 2 at strainer punching plate thickness = 8mm

The finite element analysis (FEA) findings of Geometry B of Case 1, as shown in Figure 13, indicate significant patterns in the structural response of the tapered constituent at strainer punching plate thickness = 8 mm. Actual condition is hereby referred to as (Case 1). Simulating contingency is a common practice to account for uncertainties and to identify potential risks and weaknesses in the current design. Therefore, the actual condition with 20% increase in fluid temperature and pressure is hereby referred to as (Case 2).

The von Mises stress plot shows that the stresses are the highest at the narrow tip of the geometry, where the area of cross-section is the smallest. This is anticipated since narrowing of the material width causes the load exerted to be concentrated on a smaller region, which increases the stress field in the region. The level of stress reduces by a large percentage as the geometry is opened up towards the base, and this shows that the bigger cross-section is more efficient in the redistribution of the load applied. There are small localised peaks of stress running along the mid-section; this could either be due to geometric transitions or local stiffness variation, although these cannot be found to exceed the critical levels found at the tip. By and large, the stress field indicates that the constriction end of the structure is the weakest in yielding or collapsing under the loading condition of the load.

This observation is also confirmed by the plot of displacement, as it shows that the highest displacement is at the same narrow tip of the geometry. Since the stiffness also depends on the cross-sectional sizes, the tapering shape gives inherent higher flexibility to the free end. This causes the displacement to flow smoothly at the base, where the deformation is minimal, since the structure is bound to the tip, whereby the structure is in the highest degree of total deflection. The displacement distribution means that though the component is expected to behave in a certain way when it is under load, the tip part might have an unwanted movement according to the demands of operation. Sometimes the design needs to be stiff or geometrical improvements made to ensure high positional accuracy, vibration resistance or low deflection.

The distribution of strains that would represent deformation when compared to the original shape of the material follows a similar pattern to the stresses. The maximum values of strain are concentrated at the tapered end. This implies that the area experiences maximum deformation under the force applied. As the strain is directly proportional to stress due to the elastic properties of the material, these findings prove that the tip is the most important part of it in terms of possible material stretching or even permanent deformation. Most of the other geometry is relatively low strain, indicating that most of the structure has safe elastic limits during the loading process.

In conclusion, the von Mises stress, displacement, and strain plots all tend to point at the narrow tip as the crucial area of the design of Geometry B within Case 1. It is the region where the mechanical demand is the highest and thus is the most probable location of failure initiation or excessive deformation. In engineering terms, the outcomes indicate that engineering enhancements, including making the tip thicker, changing the taper profile, or a change in the choice of materials, can be useful to improve performance and reliability. These results give a good indication of how the further optimisation of the component can be done under the stated loading conditions.

The FEA outputs of Geometry B in Case 2, as shown in Figure 14, present a pattern of structural response that is in line with the tapered nature of the component, but there is a considerable difference in magnitude to Case 1 at strainer punching plate thickness = 8 mm. Actual condition is hereby referred to as (Case 1). Simulating contingency is a common practice to account for uncertainties and to identify potential risks and weaknesses in the current design. Therefore, the actual condition with 20% increase in fluid temperature and pressure is hereby referred to as (Case 2). The von Mises stress distribution once

Item	FEA Plot
vonMises Stress	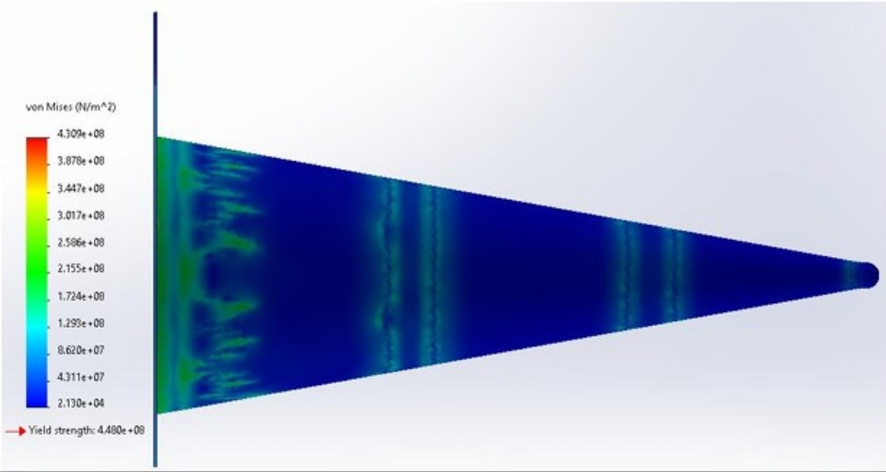
Displacement	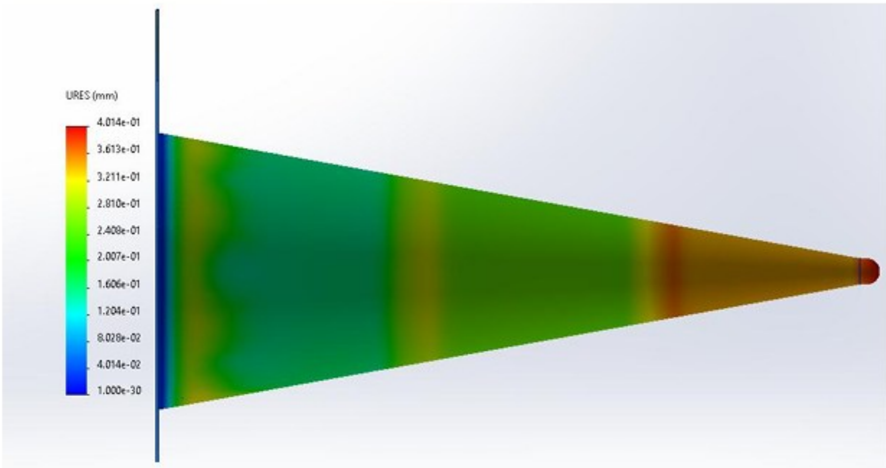
Strain	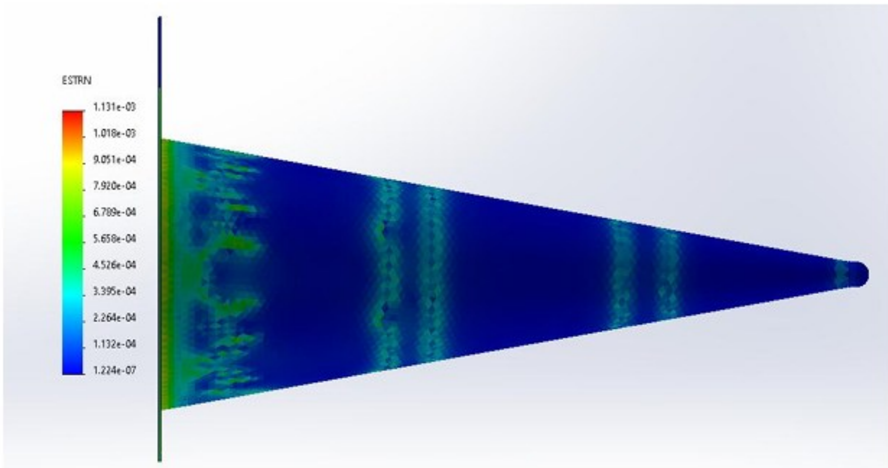

Figure 13. The FEA plot for Geometry B – Case 1 reveals that maximum stress, displacement, and strain are concentrated at the tapered tip, identifying it as the critical structural weakness under normal operating conditions.

again indicates that the greatest stresses are located close to the narrowing tip of the geometry, though the stresses seem to be a little lower compared to the level in Case 1. This implies that loading or boundary conditions in Case 2 lead to the creation of a less intense stress concentration at the tip. The broader base still portrays the low stress and shows that there is a good distribution of the load over the expanded cross-sectional area. The localised stress variations are also observed in the middle section, and these could be due to the mesh density or some slight variations in stiffness in the taper. Overall, the stress field reveals that although the tip is the most imperative area, the structure with Case 2 has a slightly better stress behaviour compared to Case 1.

Case 2 displacement plot takes the expected trend of deformation of a tapered structure, with the narrow, free end experiencing the most displacement. Nevertheless, the extent of displacement seems to be a bit smaller in comparison to the last one, which means a possibly smaller load applied as well as a different direction of loading or other support conditions. Displacement gradient in the case is a gradual decrease of the fixed base, where movement is minimal at the tip, where flexibility is the highest. This strengthens the fact that a tapered profile would automatically lead to higher deflection in the part of the structure that is narrowest. Although the movement at the tip is still substantial, its decrease in comparison with Case 1 indicates that Case 2 could be less challenging in loading or a better structural arrangement.

The strain plot shows similar tendencies to the stress plot and displacement plot. The greatest values of strain are, again, concentrated at the tip, as is in line with the area of maximum deformation and a minimum of stiffness. The strains are seen to be generally lower as compared to case 1, meaning that there is less stretch or distortion of the material in this case. Most of the geometry, especially at the base, is kept in the low-strain regions, meaning that a significant part of the component is working well in its elastic range. This trend validates the fact that the general structural reaction in Case 2 is, to some extent, reduced compared to Case 1, with the decreased material deformation along the length of the part.

Overall, the FEA plots of the Case 2 Geometry B reveal that the critical part is the slender end of the tapered structure, at which all the stress, displacement, and strain are maximised. But as compared to Case 1, the values of these reactions are significantly smaller, showing an increase in the structural performance within the circumstances prescribed to Case 2. This implies that the loading situation in Case 2 is milder or favourable to the geometry. These findings offer valuable conclusions to optimise the design by demonstrating that any change in the load conditions or constraints in the support or the operating conditions can dramatically affect the mechanical behaviour of the component. Should the need arise, both cases can be compared quantitatively or determined whether the observed process of eliminating stress and deformation is within acceptable design limits.

Von mises stress, displacement and strain of geometry C of the case 1 and case 2 at strainer punching plate thickness = 10 mm

The FEA output of Geometry C with Case 1, which is illustrated in Figure 15 at strainer punching plate thickness = 10 mm, has a structural response that is highly predictable as far as a tapered geometry is concerned, but has a few different features in relation to Geometry B. Actual condition is hereby referred to as (Case 1). Simulating contingency is a common practice to account for uncertainties and to identify potential risks and weaknesses in the current design. Therefore, the actual condition with 20% increase in fluid temperature and pressure is hereby referred to as (Case 2). Stress distribution on the component (von Mises) reveals that the maximum stress comes at the sharp, narrow end of the component, where the cross-section of the material is minimal. This stress concentration is directly related to the geometric constraint, in that the load is passed through an area which is shrinking as the taper continues. Consequently, the stress levels shoot up at the tip as indicated by the red and orange curves in the figure. Towards the broader base, the stresses reduce by a significant factor, which supports the idea that the broader area will be able to spread the

Item	FEA Plot
vonMises Stress	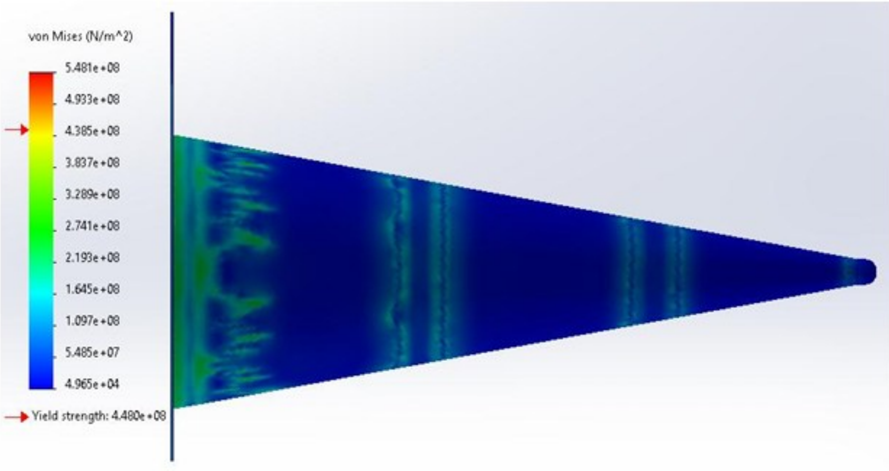
Displacement	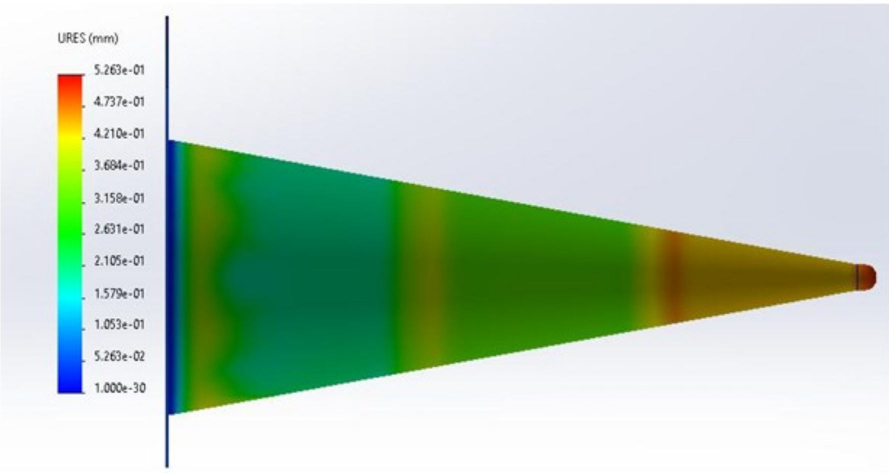
Strain	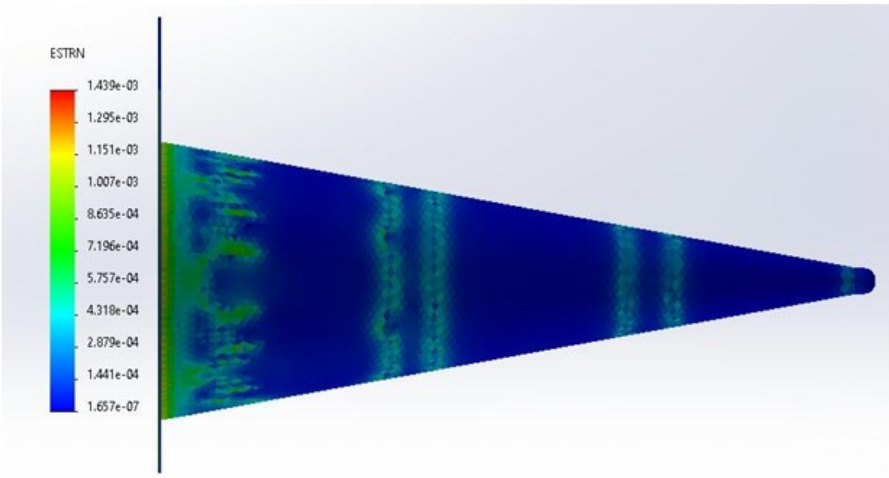

Figure 14. The FEA plot for Geometry B – Case 2 displays reduced stress and deformation compared with those in Case 1, indicating improved structural response under contingency operating conditions, although the tip remains the most critical region.

load more effectively. Minor differences in the midsection can be explained by the fact that the transition to the material stiffness or the pattern of the nets can occur, but it is not that significant in comparison with the sharp concentration of stress at the tip. The displacement plot also shows the mechanical behaviour of Geometry C in Case 1. The highest displacement would be at the slender free end of the geometry, which is the least stiff. This is in line with the deformation pattern of a tapered structure under external forces, as to be expected. The distribution of the displacement is a smooth transition between small values at the fixed base to larger values towards the tip with a predictable gradient. In comparison with the strains seen, the displacement is significant, and it is validated that the narrow portion of the tip to which the component is attached is the most flexible and dynamic. Although this deformation might not be a problem based on the application, a lot of movement in the tip may be a problem with the components that need high accuracy, less vibration, or stability under the load.

Strain distribution shows the same trend as the stress and displacement fields. The parts that have the highest strains are the parts where high levels of stress and deformation are observed, especially at the tapered end. This implies that the local deformation is the highest at this point, as the cross -section is smaller and the intensity of stress is higher. The rest of the geometry indicates quite low strain values, and this indicates that the greater portion of the structure is well within its elastic limits as long as it is being loaded. The strain gradient is gradual along the length a consequence of the natural occurrence of the variation in stiffness of tapered shapes.

In conclusion, the FEA plots of Geometry C of Case 1 indicate that the thin tip of the structure is the problematic area, and the maximum stress, displacement, and strain take place in it. The broader base works well with low deformation and low stress levels. These findings demonstrate that the tip area should be assessed with regard to the possibility of failure, fatigue, or over-deformation due to operational loads. Where necessary, modifications to the design, like thickening of the tip, changing the taper shape, or choosing a material that is more rigid, may enhance mechanically. The results provide useful information on Geometry C behaviour to load distribution and can be used to improve designs to achieve improved reliability and durability.

Figure 16 of the FEA results of Geometry C under Case 2 at strainer punching plate thickness = 10 mm shows that the structural behaviour of Case 2 is closely similar to that of Case 1, with significant decreases in the magnitude of stress and deformation. Actual condition is hereby referred to as (Case 1). Simulating contingency is a common practice to account for uncertainties and to identify potential risks and weaknesses in the current design. Therefore, the actual condition with 20% increase in fluid temperature and pressure is hereby referred to as (Case 2). Using von Mises stress distribution, it is seen that the maximum stress values are again concentrated at the slender end of the tapered geometry, as is to be expected by the geometrical effect of stress concentration occurring where there is the least cross-sectional area. Nonetheless, the overall stress levels seem to be slightly reduced compared to those in Case 1, and this indicates that in Case 2, the load or boundary conditions exert a weaker stress state on the component. The broader base still demonstrates the very low values of stress, which proves load-bearing character of the main one. The slight differences in stress intermediate through the midsection indicate the natural shifts of hardness along the taper, but these are still far less than critical values. Overall, the stress field demonstrates that despite the tip being the most susceptible part of the structure, the stress distribution becomes more favourable than in the previous example.

The distribution of displacement follows the same pattern as well, revealing that the most deformation occurs at the narrow and free end of the geometry. This is not surprising because the tip is the least rigid and hence the most sensitive to the forces exerted on it. The displacement reduces slowly to the fixed base so that there is a smooth gradient of high to low deformation. The level of displacement across the structure is slightly lower

Item	FEA Plot
vonMises Stress	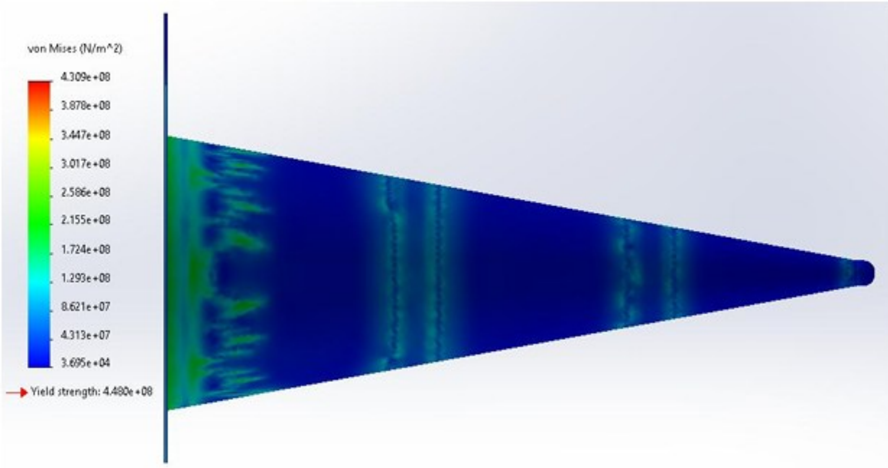
Displacement	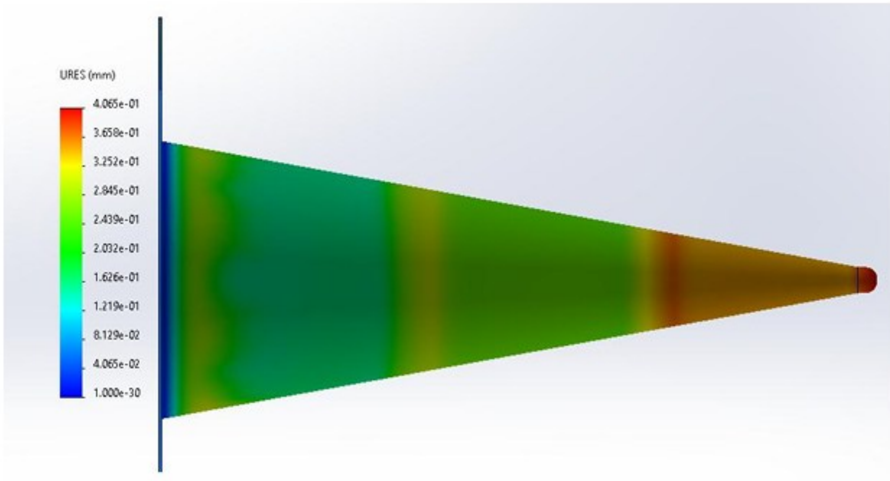
Strain	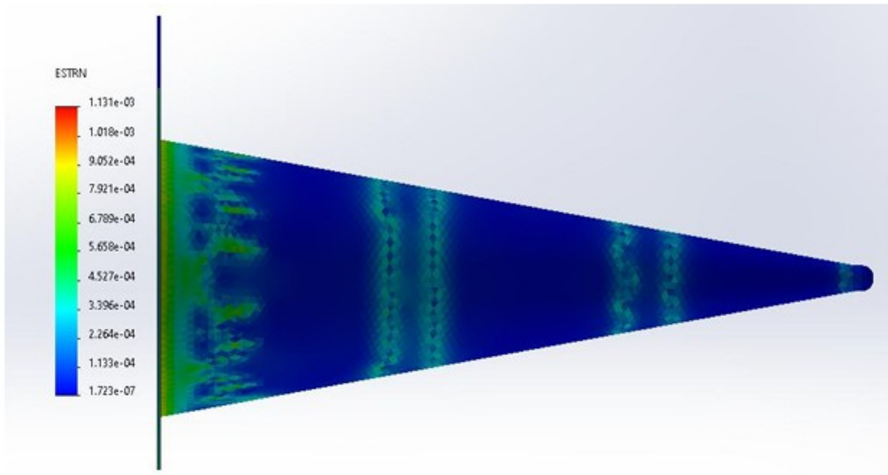

Figure 15. The FEA plot for Geometry C – Case 1 highlights significant stress concentration and deformation at the tapered tip, confirming it as the primary failure-prone region despite overall stable structural behavior.

than in Case 1, suggesting that in Case 2, the component is not subjected to as much total demand in terms of deformation. This decrease might be an indication of a better loading setup or a `more favourable structural support environment. Although this has reduced, the tip is still the most displaced area, and on application, may need to be considered in case excessive movement may influence performance, alignment or vibration behaviour.

The distribution of the strain is more or less similar to the trend in the results of stress and displacement. The maximum strain values are at the tapered end, where the material deformation is the most, since the cross-section is lower and the local stress intensity is higher. It would seem that the strain is not as large as in Case 1, and it supports the idea that Case 2 is a less serious loading environment. The rest of the structure, especially in the broad base, showed low degrees of strain, which was well within the elastic range of the material. This implies that the majority of the geometry is safe in the conditions it is in, and only the tip achieves significant deformation.

In conclusion, the FEA outcomes of Geometry C of Case 2 indicate that the narrow tip is the most important area with regard to the response of stress, displacement, and strain. Nevertheless, these magnitudes of these responses are always smaller than the ones in Case 1, which means that the structural behaviour has improved in the Case 2 loading scenario. This implies that Case 2 can reflect a more realistic, optimised or even less severe operating environment. These results represent a good contribution to the understanding of how the load arrangement and boundary conditions can affect the tapered geometries' performance and may be used to refine future design. As an example, in case additional reduction of tip deformation or stress concentration is needed, adjustment of the tip thickness, taper angle, or material reinforcement could be considered.

UC values for different geometries

The values of Punching Plate UC provided in Geometries A, B, and C in Case 1 and Case 2, as shown in Table 8, highlight the structural adequacy of each configuration in the conditions of loading provided. The UC value is a ratio of the effect of the applied load to the allowable load capacity, where anything below 1.0 of the standard is considered to be structurally acceptable (OK) and anything above 1.0 (NG - Not Good). Based on the findings, it is clearly seen that the performance of Geometry A is low in both cases, with UC values of 1.14 in Case 1 and 1.47 in Case 2. These values are higher than the permissible limit, which implies that Geometry A is always overstressed and unable to safely oppose the loads applied to it. This implies that Geometry A, as designed, does not suffice based on the design characteristics of the geometry, be it its shape, thickness, load distribution characteristics, etc.

Conversely, Geometry B depicts both good and poor performance, whereby the UC in Case 1 is 0.90, which is within acceptable ranges, thus rated safe. In Case 2, however, UC goes up to 1.14, which is above capacity, and the effect is an "NG! designation. This means that Geometry B is also sensitive to the change that has been imposed in Case 2, like the change in loading or the boundary conditions. The fact that the 0.90 has changed to 1.14 indicates that Case 2 sets out towards a more demanding or unfavourable loading scenario, which causes the structure to exceed its allowable stress limit. Although Geometry B can be adequate in a given set of conditions, it is not consistent, which leaves its applicability to be questioned in case of situations where loading can be unstable.

Geometry C shows the best structural performance when compared to the other two designs. Both UC values of 0.75 in Case 1 and 0.96 in Case 2 do not exceed the acceptable level, showing that the geometry is structurally safe in both cases of loading. The values also indicate that Case 1 shows that Geometry C has a comfortable margin of safety, whereas Case 2 shows that it is close to the threshold, although not over it. Geometry C proves to be a stronger trend, which can support a more intense load than Geometries A and B. The geometry of the C shape and stress distribution tendencies seems to give the Geometry C a superior resistance to localised punching forces, and it is thus the most feasible choice in regard to structural capacity.

<table>
<tr><th>Item</th><th>FEA Plot</th></tr>
<tr><td>vonMises Stress</td><td>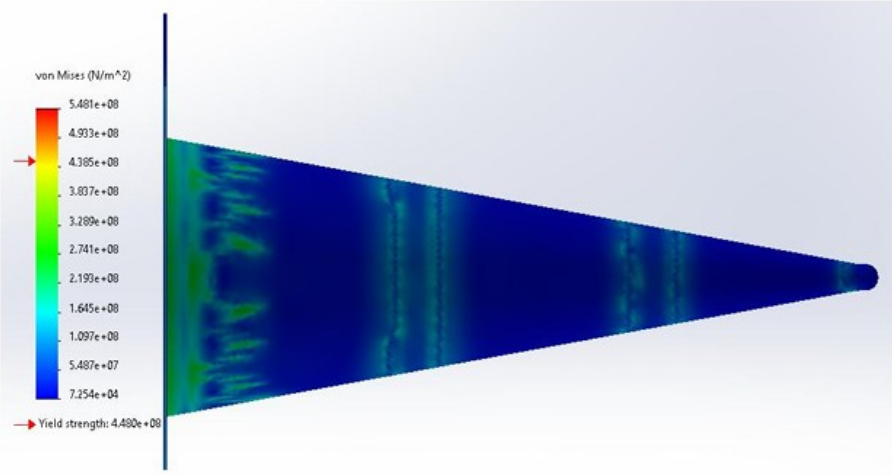
</td></tr>
<tr><td>Displacement</td><td>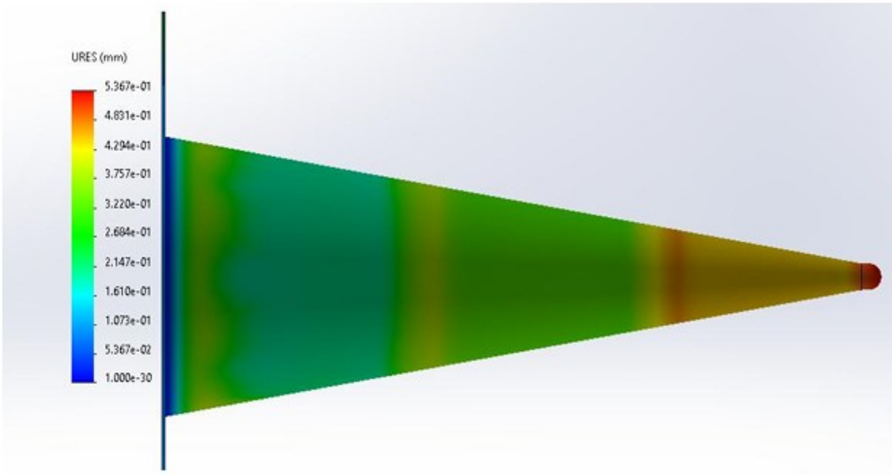
</td></tr>
<tr><td>Strain</td><td>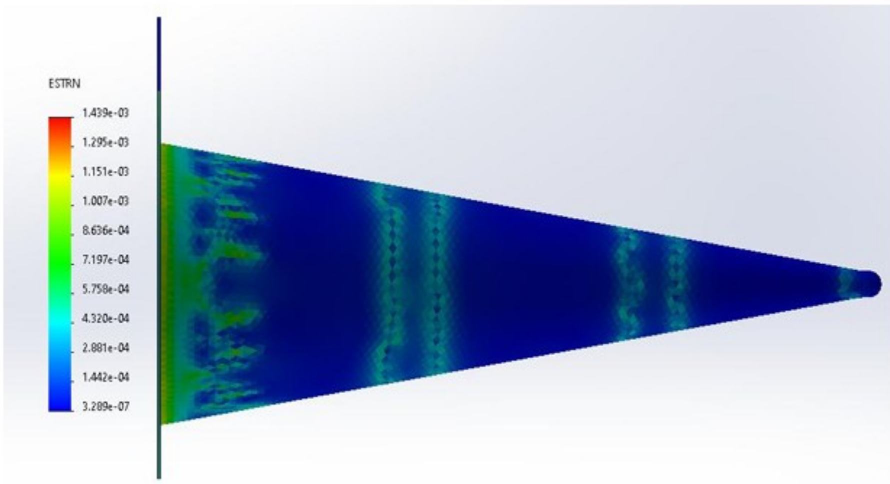
</td></tr>
</table>

Figure 16. The FEA plot for Geometry C – Case 2 shows improved structural response with lower stress and deformation compared with those in Case 1, while still identifying the tapered tip as the primary critical region.

Table 8. UC values for different geometries

Geometry	Case	Punching plate UC	Remarks	Maximum pressure drop (Pa)
A	1	1.14	NG!	6794.1127
	2	1.47	NG!	10610.3041
B	1	0.9	OK!	7363.4831
	2	1.14	NG!	10552.3552
C	1	0.75	OK!	7201.3949
	2	0.96	OK1	10579.5611

On comparing the geometries as a whole, it is evident that Geometry C has the best structural performance, followed by Geometry B, which is not so good in either of the two cases. Geometry A is the one that constantly fails the punching plate test and will have to undergo a considerable redesign to comply with safety regulations. These values of UC can be used to understand how well each geometry would work and how reliable it would be under different operating conditions, which may be used quantitatively to decide between which design is most effective under different operating conditions and which design should be optimised or implemented.

CONCLUSION

In conclusion, this study investigated the structural integrity and hydraulic performance of low-temperature separation unit (LTSU) strainers using a coupled Computational Fluid Dynamics (CFD) and Finite Element Analysis (FEA) approach. The analysis successfully identified the root cause of failure in the original design (Geometry A), which was primarily excessive stress concentration at the handle–plate junction under fluid-induced loading. The results demonstrate that insufficient punching plate thickness significantly compromises structural integrity, particularly under contingency operating conditions.

From a hydraulic perspective, all modified geometries (B and C) resulted in an increased pressure drop compared with the baseline. However, the increase remained within an acceptable range, indicating that structural improvements can be achieved without severely compromising flow performance. Structurally, Geometry C (10 mm thickness) exhibited the best structural performance, maintaining unity check (UC) values within allowable limits under both normal and contingency operating conditions, while significantly reducing stress concentration, deformation, and strain.

From an operational perspective, the findings highlight that minor design modifications, particularly increasing punching plate thickness, can substantially enhance equipment reliability and prevent premature failure in LTSU systems. This provides direct benefits for oil and gas operations, including reduced maintenance frequency, improved operational safety, minimized unplanned downtime, and enhanced protection of downstream equipment from debris contamination.

The novelty of this study lies in the integrated CFD–FEA framework used to directly link fluid-induced pressure loads with structural response for failure diagnosis and design optimization of LTSU strainers. Unlike conventional approaches that treat hydraulic and structural analyses separately, this study provides a comprehensive evaluation of fluid–structure interaction effects under both normal and contingency conditions, offering a more realistic representation of operational behavior.

For future research, it is recommended that transient and cyclic loading conditions be incorporated to evaluate fatigue life more accurately, as well as to investigate the effects of material variability and weld quality on failure initiation. Additionally, experimental validation of the simulation results and inclusion of multiphase flow behavior, such as wax deposition and particle accumulation, would further enhance the reliability and applicability of the findings.

ACKNOWLEDGEMENT

Communication of this research is made possible through monetary assistance by Universiti Tun Hussein Onn Malaysia, UTHM Publisher's Office via Publication Fund E15216 and this research was also supported by Universiti Tun Hussein Onn Malaysia (UTHM) Research Management Centre (RMC) provided through the GPPS (vot J053).

DECLARATIONS

Author Contribution

Mohd Azni Md Kasim, Mohd Azahari Razali, Norfakhira Mohd Nor, Iman Fitri Ismail, Masataro Suzuki, and Amnur Akhyan contributed equally as the main contributors of this paper. All authors read and approved the final version of the manuscript.

Funding Statement

None

Competing interest

None

The use of AI or AI-assisted technologies

None

GLOSSARY OF TERMS AND SYMBOLS

Terms & Symbols	Definition	Unit
ΔP_i	Total initial pressure drop	Pa
d	Pore diameter	mm
Cp/Cv	Specific heat ratio	-
Cp	Specific heat	J/kg*K
AR	Aspect ratio	-
UC	Unity check	-

REFERENCES

Adrianto, A., Syihab, Z., Marhaendrajana, T., & Sutopo, S., (2025), A Hybrid Probabilistic-Backpropagation Neural Network Solver for Nonlinear Systems in Reservoir Simulation. *Scientific Contributions Oil and Gas*, 48(3), 31-40. https://doi.org/10.29017/scog.v48i3.1751.

Amnur Akhyan, Hussein, M. D., & Mohd., (2025), Influence of Installation Orientation and Cone Angle on Pressure Drop and Filtration Efficiency of Conical Strainers. *Scientific Contributions Oil and Gas*, 48(3), 303–320. https://doi.org/10.29017/scog.v48i3.1910.

Akhyan, A., Bin Razali, M. A., Hendriko, Mahzan @ Mohd Zin, S. B., & Bin Ismail, I. F., (2025), Porosity-Controlled Flow Instability and Vibration Response in Conical Strainers: An Integrated Hydraulic-Structural Evaluation. *Scientific Contributions Oil and Gas*, 48(4), 309 –321. https://doi.org/10.29017/scog.v48i4.1960.

Amirante, D., Hills, N. J., & Barnes, C. J., (2012), Thermo-Mechanical Finite Element Analysis/ Computational Fluid Dynamics Coupling of an Interstage Seal Cavity Using Torsional Spring Analogy. Journal of Turbomachinery-Transactions of The Asme, 134(5), 051015. https://doi.org/10.1115/1.400425.

Bakker, andre, & Marshall, elizabeth m. (n.d.). Computational Fluid Dynamics. https://doi.org/10.31399/asm.hb.v20.a000244

Beattie, D. L. G., Bear, H., & Willis, R. B., (1983), Pipeline concave strainer. https://www.freepatentsonline.com/4543114.htm.

Bruchet, P., & Kanno, A., (2019), Strainer and straining system.

Carlomagno, M., Rossin, S., Delvecchio, M., & Anichini, A. (2012, June). Experimental and numerical validation of conical strainer fluid/ structural performance model. In Turbo Expo: Power for Land, Sea, and Air (Vol. 44724, pp. 155-171). American Society of Mechanical Engineers. https://doi.org/10.1115/gt2012-6975.

Currence, K. L., (2016), Enhanced low temperature separation process. https://www.freepatentsonline.com/y2017/0122658.htm.

Chen, S., Jin, X., Hu, R., Liu, F., & Hu, Z., (2023), Investigation on the Rock-Fragmentation Process of Conical-Shaped TBM Cutterhead in Extremely Hard Rock Ground. Stavební obzor-

Civil Engineering Journal, 32(3), 409-425. https://doi.org/10.14311/cej.2023.03.003.

Computational fluid dynamics. (n.d.). https://doi.org/10.1007/978-3-319-30686-5_

Gao, Q., Ding, L., & Huang, D., (2019), Experimental and numerical study on loss characteristics of main steam valve strainer in steam turbine. Applied Thermal Engineering, 147, 935-942. https://doi.org/https://doi.org/10.1016/j.applthermaleng.2018.07.03.

Gülich, J. F., (2014), Numerical Flow Calculations (pp. 499–574). Springer Berlin Heidelberg. https://doi.org/10.1007/978-3-642-40114-5_8.

Hadebe, X. P., Tchomeni, B. X., Alugongo, A. A., & Sozinando, D. F., (2024), Finite Element Analysis and Computational Fluid Dynamics for the Flow Control of a Non-Return Multi-Door Reflux Valve. Fluids, 9(10), 238. https://doi.org/10.3390/fluids910023.

Kim, J. Y., (2009), Strainer with omega type screen.https://www.freepatentsonline.com/y2009/0283463.html.

Kurochkin, A. V., (2020), Low-temperature fractionation unit for complex gas treatment and production of lng.

Rea, D. B., Mann, A. B., Hornyak, R. F., & McKean, R. A., (1984), In-line pipeline strainer. https://www.freepatentsonline.com/4582605.htm.

Richter, J. R., & Martin, R. I., (2017), Pipeline strainer for reducing entrained gas and debris.https://www.freepatentsonline.com/y2017/0299107.htm.

Kurochkin, A. V., (2019), Apparatus for low-temperature dephlegmation with separation of ltds for preparing natural gas to obtain an ethane -butane fraction and method of operation thereof.

Kurochkin, A. V., (2019), Plant of low-temperature separation with fractionating absorption ltsfa for processing of natural gas with extraction of hydrocarbons (versions).

Li, W., Ji, L., Agarwal, R. K., Shi, W., & Zhou, L. (2024). Brief Review of Computational Fluid Dynamics (pp. 21–46). Wiley. https://doi.org/10.1115/1.862mfp_ch.

Li, J., Zhang, H., Davis, G., Kalb, F., & Hamid, S. (n.d.). Improving the Closing Characteristics of Subsurface Safety Valve with Combined FEA and CFD Modeling/Numerical Analysis. https://doi.org/10.2523/93941-m

Łuczyński, P., Giesen, M. P., Gier, T.-S., & Wirsum, M., (2019), Uncoupled CFD-FEA Methods for the Thermo-Structural Analysis of Turbochargers. 4(4), 39. https://doi.org/10.3390/IJTPP404003.

Mahajan, G., & Maurya, R. S. (2020). Development of an efficient t-type strainer with its performance evaluation. Journal of thermal engineering, 6(6), 4 2 0 - 4 3 3 . h t t p s : / / d o i . o r g / 1 0 . 1 8 1 8 6 /thermal.836499

Masuda, H., Iyota, H., & Ohmura, N., (2021), G l o b a l C o n v e c t i o n C h a r a c t e r i s t i c s o f Conical Taylor-Couette Flow with Shear-Thinning Fluids. Chemical Engineering & Technology, 44(11), 2049-2055. https://doi.org/10.1002/ceat.20210023.

Min, I., Choi, J., Kim, G., & Jo, H., (2024), CFD Analysis of the Pressure Drop Caused by the Screen Blockage Rate in a Membrane Strainer. Processes, 12(4), 831. https://doi.org/10.3390/pr1204083.

Nakayama, Y. (n.d.). Computational Fluid Dynamics. https://doi.org/10.1016/b978-0-08-102437-9.00015-.

Nursyifa, A., (2017), Optimalisasi Sistem Informasi Terintegrasi Dalam Meningkatkan Kinerja Penelitian dan Pengembangan Di Subsektor Minyak dan Gas (Optimizing integrated information system in improving research and development performance in subsector oil and gas). *Lembaran Publikasi Minyak Dan Gas Bumi*, 51(2), 95–100. https://doi.org/10.29017/LPMGB.51.2.20.

Odabaee, M., Modir Shanechi, M., & Hooman, K., (2014), CFD simulation and FE analysis of a high pressure ratio radial inflow turbine. 1–4. https://people.eng.unimelb.edu.au/imarusic/proceedings/19/205.pd.

Pasarai, U., Hazman, H., Pribadi, E., Lucia, A., & Widarsono, B., (2019), Kajian Regulasi Pengusahaan Oil Sands Kedalaman Dangkal Dengan Metode Oil Mining. *Lembaran Publikasi Minyak Dan Gas Bumi*, 53(1), 1–14. https://doi.org/10.29017/LPMGB.53.1.265.

Sunarjanto, D., Suliantara, S., Iskandar, U. P., & Nainggolan, M. T. P., (2014), Sistem Informasi Geogra untuk Optimasi Eksplorasi dan Pengembangan Wilayah Migas Geographic Information System for Optimization Exploration Oil and Gas Area Development. https://doi.org/10.29017/LPMGB.48.1.22.

Sunarjanto, D., Yusgiantoro, L. A., Sismartono, D., Utomo, R. B. H., & Akbar, W. A., (2017), Manfaat Ekonomi Dan Lingkungan Dari Kegiatan Migas Teluk Bintuni, Propinsi Papua Barat (The Benefit of Economic and Environment Oil and Gas Activity in Bintuni Gulf, West Papua). *Lembaran publikasi minyak dan gas bumi*, 51(3), 125-134. https://doi.org/10.29017/LPMGB.51.3.24.

Sun, Z., Chew, J. W., Hills, N. J., Volkov, K., & Barnes, C. J., (2010), Efficient Finite Element Analysis/Computational Fluid Dynamics Thermal Coupling for Engineering Applications. Journal of Turbomachinery-Transactions of The Asme, 132(3), 031016. https://doi.org/10.1115/1.314710.

Schmidt, W., (1987), Numerical Simulation of Turbulent Flows Using Navier Stokes Equations (pp. 473–497). Springer, Berlin, Heidelberg. https://doi.org/10.1007/978-3-642-82994-9_1.

Sun, Z., Chew, J. W., Hills, N. J., Volkov, K., & Barnes, C. J., (2008), Efficient FEA/CFD Thermal Coupling for Engineering Applications. 1505–1515. https://doi.org/10.1115/GT2008-5063.

Sotoodeh, K., (2019), Handling the pressure drop in strainers. Marine Systems & Ocean Technology, 14(4), 220-226. https://doi.org/10.1007/s40868-019-00063-.

Sotoodeh, K., (2019), Handling the pressure drop in strainers. Marine Systems & Ocean Technology, 14(4), 220-226. https://doi.org/10.1007/s40868-019-00063-.

Saksena, D. P., & Lakhera, V. J., (2022), Numerical study on pressure drop characteristics for turbulent flow in conical spiral tubes. Engineering Research Express, 4 (3), 035023. https://doi.org/10.1088/2631-8695/ac84c.

Shaikh, J. S., Pathan, K. A., & Khan, S. A., (2024), Numerical Simulation of Surface Pressure and Temperature Distribution Along a Cone at Supersonic Mach Numbers Using CFD. Journal of Advanced Research in Numerical Heat Transfer, 28, 1-26. https://doi.org/10.37934/arnht.28.1.12.

Sun, Z., Chew, J. W., & Hills, N. J., (2009), Use of CFD for Thermal Coupling in Aeroengine Internal Air Systems Applications (pp. 399–404). Springer, Berlin, Heidelberg. https://doi.org/10.1007/978-3-540-89749-1_6.

Zhang, J., & Xiao, Y., (2012), Low temperature separator of liquefied gas.

Zhu, L., Wang, D., Liu, G., & Liu, H., (2022), Oiling low temperature separation process for dehydration and de-hydrocarbon of natural gas and practical application. Science and Technology for Energy Transition, 77, 8. https://doi.org/10.2516/stet/202200.